Article

Molecular Cell

Metal Sensing by the IRT1 Transporter-Receptor Orchestrates Its Own Degradation and Plant Metal Nutrition

Graphical Abstract

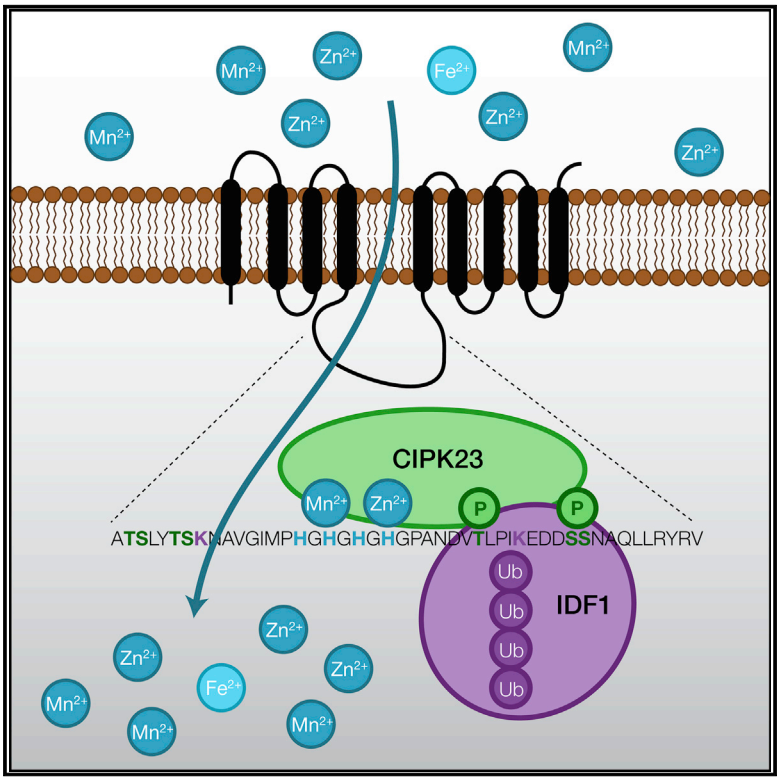

Highlights

- Soil metal excess is directly sensed by the IRT1 plant metal transporter-receptor
- CIPK23 phosphorylates metal-loaded IRT1 and triggers its K63 polyUb by IDF1
- K63 polyUb and phosphorylation are both required to target IRT1 to the vacuole
- IRT1 vacuolar degradation limits the accumulation of highly reactive metals in plants

Authors

Guillaume Dubeaux, Julie Neveu, Enric Zelazny, Grégory Vert

Correspondence

gregory.vert@i2bc.paris-saclay.fr

In Brief

Plants protect themselves from highly reactive metals found in soils by tightly regulating the localization and the abundance of root metal transporters. Dubeaux et al. now report on the ability of the IRT1 transporter to directly sense metal excess and to initiate a response that culminates in IRT1 destruction.

Dubeaux et al., 2018, Molecular Cell *69*, 953–964
March 15, 2018
https://doi.org/10.1016/j.molcel.2018.02.009

CellPress

Molecular Cell
Article

Metal Sensing by the IRT1 Transporter-Receptor Orchestrates Its Own Degradation and Plant Metal Nutrition

Guillaume Dubeaux,[1] Julie Neveu,[1] Enric Zelazny,[1] and Grégory Vert[1,2,*]
[1]Institute for Integrative Biology of the Cell (I2BC), CNRS/CEA/Univ. Paris Sud, Université Paris-Saclay, 91198 Gif-sur-Yvette, France
[2]Lead Contact
*Correspondence: gregory.vert@i2bc.paris-saclay.fr
https://doi.org/10.1016/j.molcel.2018.02.009

SUMMARY

Plant roots forage the soil for iron, the concentration of which can be dramatically lower than those needed for growth. Soil iron uptake uses the broad metal spectrum IRT1 transporter that also transports zinc, manganese, cobalt, and cadmium. Sophisticated iron-dependent transcriptional regulatory mechanisms allow plants to tightly control the abundance of IRT1, ensuring optimal absorption of iron. Here, we uncover that IRT1 acts as a transporter and receptor (transceptor), directly sensing excess of its non-iron metal substrates in the cytoplasm, to regulate its own degradation. Direct metal binding to a histidine-rich stretch in IRT1 triggers its phosphorylation by the CIPK23 kinase and facilitates the subsequent recruitment of the IDF1 E3 ligase. CIPK23-driven phosphorylation and IDF1-mediated lysine-63 polyubiquitination are jointly required for efficient endosomal sorting and vacuolar degradation of IRT1. Thus, IRT1 directly senses elevated non-iron metal concentrations and integrates multiple substrate-dependent regulations to optimize iron uptake and protect plants from highly reactive metals.

INTRODUCTION

Plants are fixed organisms that must constantly monitor their outside environment and adjust their growth and development for survival (Vert and Chory, 2011). The acquisition of nutrients from the soil is absolutely essential for plant development. Among them, iron is of the utmost importance because of its ability to change redox states, making it an indispensable cofactor in electron transport chains and catalytic processes (Briat et al., 1995). This essential role of iron is highlighted by the severe disorders promoted by its deficiency, such as anemia in mammals or chlorosis and yield loss in plants (Briat et al., 1995). Although abundant in nature, iron is often poorly available in soils because it is found in rather insoluble ferric complexes. Dicotyledonous plants, such as the model plant *Arabidopsis thaliana*, rely on a multistep iron uptake strategy involving rhizosphere acidification, reduction of iron, and transport inside root epidermal cells using the ferrous iron transporter IRT1 (Eide et al., 1996; Vert et al., 2002). An *irt1* loss-of-function mutant is severely chlorotic and dies early in development, unless fertilized with massive amounts of iron (Vert et al., 2002). Iron absorption into root peripheral cells by IRT1 is therefore critical for proper plant iron nutrition and establishment of iron homeostasis. IRT1 is a broad-spectrum transporter, driving the uptake in plants of non-iron essential heavy metals required in minute amounts such as manganese, zinc, and cobalt, as well as the uptake of toxic cadmium ions (Barberon et al., 2011; Vert et al., 2002). The *irt1* mutant fails to accumulate manganese, zinc, and cobalt, but these do not contribute to its chlorosis and growth defects (Vert et al., 2002). This indicates that iron is the primary substrate of IRT1, and non-iron metals only secondary substrates resulting from its poor selectivity. These non-iron heavy metals are naturally present in soils, but geologic and anthropogenic activities increase the concentration of these elements in the environment to amounts that may be harmful to both plants and animals.

To meet the plant demand in iron, the root iron uptake machinery is tightly regulated at the transcriptional level by endogenous and exogenous cues (Brumbarova et al., 2015). In particular, *IRT1* promoter activity is strongly and rapidly induced upon iron limitation by direct binding of the heterodimer between FIT and two other *Arabidopsis* bHLH transcription factors from subgroup Ib (Brumbarova et al., 2015). More recently, several factors post-translationally controlling IRT1 emerged and made of IRT1 one of the model plant plasma membrane (PM) protein to study the intricate mechanisms of endocytosis in plants (Barberon et al., 2011, 2014; Ivanov et al., 2014; Shin et al., 2013). Multi-monoubiquitination was shown to control the internalization of IRT1 from the cell surface to early endosomes (EEs) (Barberon et al., 2011). A non-ubiquitinatable IRT1 variant, in which two lysine (K) residues (K159 and K174) are mutated to arginines (R), accumulates to the outer PM domain facing the soil and leads to uncontrolled metal uptake and plant death. The ubiquitin (Ub)-mediated endocytosis of IRT1 therefore appears as a crucial mechanism controlling the distribution of IRT1 in the cell and iron uptake. The IDF1 RING E3 ligase interacts with IRT1 and was proposed to destabilize IRT1 protein in the cell (Shin et al., 2013), although its biological significance remains elusive. The FYVE1 protein directly interacts with IRT1 and Ub

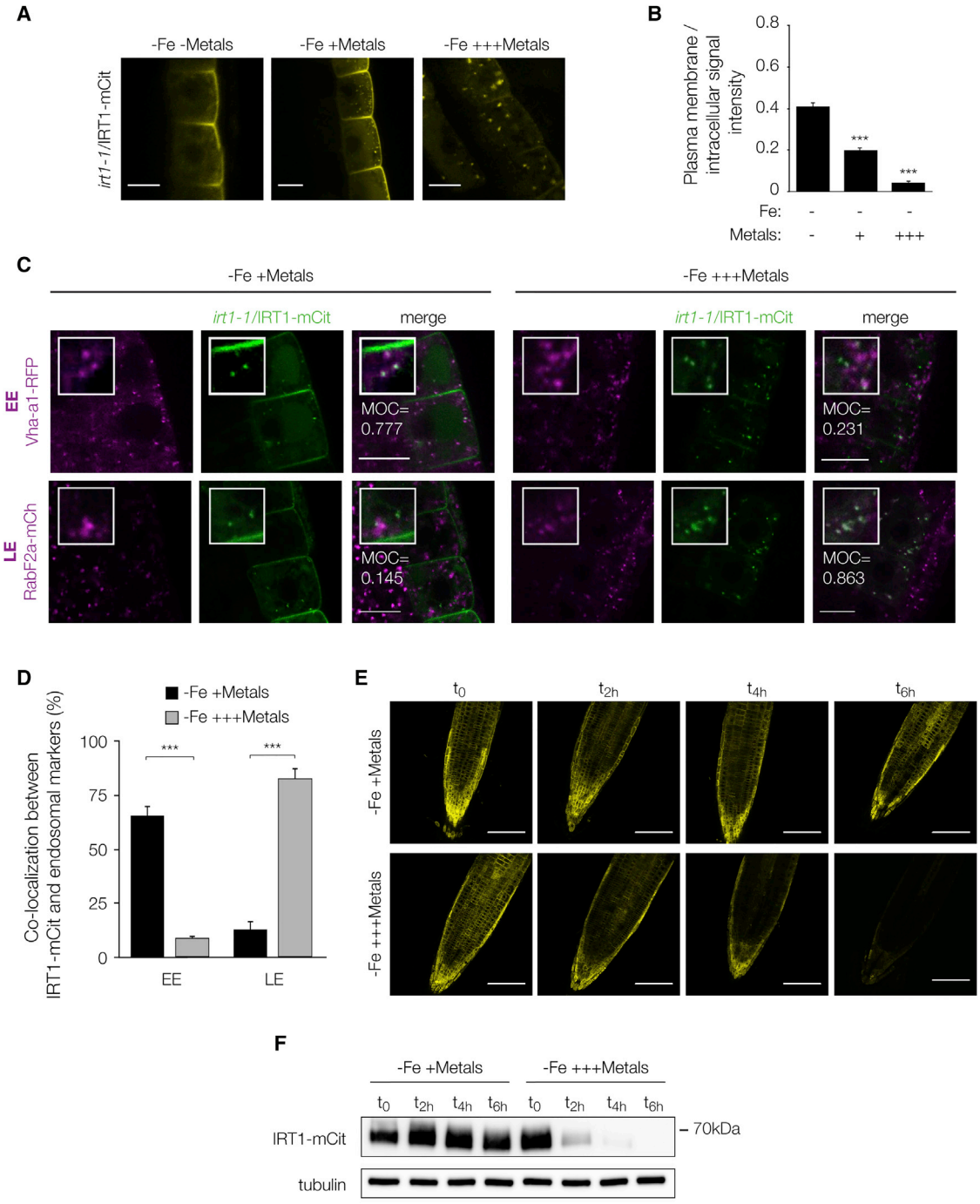

Figure 1. Non-iron Metal Substrates of IRT1 Regulate Its Localization in Root Epidermal Cells

(A) Confocal microscopy analyses of root epidermal cells from *irt1-1*/IRT1::IRT1-mCit plants grown in iron-deficient conditions and subjected to various non-iron metal regimes (Zn, Mn, and Co). Non-iron metal excess was applied for 2 days. Scale bars, 10 μm.

(B) Ratio of *irt1-1*/IRT1-mCit plasma membrane (PM) to intracellular signal intensities from experiments performed as in (A). Experiments were carried out in triplicates on stacks encompassing epidermal cells. Error bars represent SD (n = 18). The asterisks indicate significant differences to –Fe –Metals (one-way ANOVA, Dunnett post-test, $p < 0.0001$).

(C) Co-localization of *irt1-1*/IRT1-mCit with EE (Vha-a1-RFP) or LE (RabF2a-mCherry) markers. Non-iron metal excess was applied for 2 days. MOC, Mander's overlap coefficient.

(legend continued on next page)

and is recruited to the endosomal sorting complex required for transport (ESCRT) in late endosomes (LEs) (Barberon et al., 2014; Gao et al., 2014). FYVE1 was shown to be required for the sorting and the vacuolar targeting of several plant ubiquitinated cargos (Barberon et al., 2014; Belda-Palazon et al., 2016; Gao et al., 2014; Kolb et al., 2015). Surprisingly, interference with *FYVE1* expression leads to apolar localization of IRT1 at the PM and is associated with impaired radial transport of metals toward the root vasculature (Barberon et al., 2014). This greatly contrasts with the outer lateral polarity observed when ubiquitination or clathrin-mediated endocytosis are impaired (Barberon et al., 2014). This indicates that endosomal sorting of IRT1 is essential for its proper partitioning in the cell. Retrieval of IRT1 from endosomes and recycling to the cell surface also requires the SNX1 protein (Ivanov et al., 2014).

To date, the Ub-mediated endocytosis of IRT1 appears as a constitutive mechanism controlling the turnover of IRT1. Neither the levels, nor the localization of IRT1 are indeed regulated by iron availability (Barberon et al., 2011), raising the question about the biological relevance of IRT1 ubiquitination. Here, we demonstrate that IRT1 acts as a transceptor, directly sensing non-iron metals using a histidine-stretch in IRT1, and regulates its own degradation by differential ubiquitination upon metal stress. Whereas multi-monoubiquitination drives IRT1 internalization from the cell surface to EE under standard growth conditions (Barberon et al., 2011), we show that non-iron metal excess triggers the extension of multimonoUb into K63 polyUb chains and promotes IRT1 vacuolar targeting. Direct metal binding to IRT1 allows the recruitment of the CIPK23 kinase and subsequent phosphorylation of IRT1. This in turns creates a docking site and facilitates the recruitment of the IDF1 E3 Ub ligase, responsible for the extension of multimonoUb moieties into K63-linked polyUb chains. Both K63 polyUb chains decorating IRT1 and CIPK23-dependent phosphorylation are required for the proper sorting and vacuolar degradation of IRT1. Altogether the dual regulation of IRT1 at the transcriptional and post-translational levels by its different metal substrates are integrated to maximize iron uptake while limiting the absorption of highly reactive and potentially toxic non-iron metals.

RESULTS

Local Non-iron Metal Availability Regulates IRT1 Subcellular Localization

The metal transport spectrum of the IRT1 iron transporter also includes manganese, zinc, cobalt, and cadmium (Eide et al., 1996; Korshunova et al., 1999; Rogers et al., 2000; Vert et al., 2001). These highly reactive non-iron metals are aspecifically transported by IRT1 upon iron limitation and accumulate to toxic levels in plant tissues (Vert et al., 2002). The subcellular localization of IRT1 protein in plants was previously investigated by immunofluorescence analyses in differentiated *Arabidopsis* root epidermal cells using anti-IRT1 antibodies (Barberon et al., 2011, 2014) or using transient overexpression of a translational IRT1 fusion with GFP in tobacco leaves (Ivanov et al., 2014). To investigate the spatial and temporal regulation of IRT1 by the availability of its non-iron metal substrates, we first generated a transgenic line expressing a functional fusion of IRT1 protein to the yellow fluorescent protein (YFP) variant mCitrine (mCit), under the control of *IRT1* promoter in the *irt1-1* mutant background. Insertion of mCit in the extracellular loop between transmembrane domain (TM) 1 and TM2 of IRT1, after residue 43, yielded a functional IRT1-mCit fusion protein as attested by the complementation of *irt1-1* growth defects and chlorosis (Figure S1A). The *IRT1* promoter drove IRT1-mCit expression in the root epidermis in response to iron deficiency, including peripheral cells from the meristem that are well suited to track the precise localization of PM proteins (Figure S1B).

To decipher the impact of non-iron metal substrates on IRT1 localization, IRT1-mCit-expressing plants were grown on media lacking iron, to activate the *IRT1* promoter, and containing different concentrations of non-iron metals. Under physiological non-iron metal provision, typically found in plant growth medium (Murashige and Skoog, 1962) and hereafter called standard growth conditions (–Fe +Metals), IRT1-mCit protein was found at the PM and in intracellular vesicles (Figure 1A), which likely correspond to EE where IRT1 was previously observed (Barberon et al., 2011). In the combined absence of Zn, Mn, and Co (–Fe –Metals), IRT1-mCit mostly accumulated at the outer PM domain directly facing the medium (Figures 1A and 1B). To further evaluate the influence of non-iron metal nutrition on IRT1-mCit localization, we transferred 10-day-old plants grown under standard metal conditions for 2 days in a medium containing a 10-fold excess of Zn, Mn, and Co (–Fe +++Metals). These conditions triggered the depletion of IRT1-mCit from the cell surface and its accumulation in large intracellular vesicles (Figures 1A and 1B). This metal-dependent change in localization is specific of IRT1 since another root cell-surface protein, such as the boron transporter BOR4, failed to respond (Figure S1C). To decipher the nature of the non-iron metal(s) driving the change in IRT1-mCit localization, we added a 10-fold excess of Zn, Mn, and Co separately. Both Zn and Mn triggered the depletion of IRT1-mCit from the cell surface and accumulation in intracellular vesicles, whereas Co had very little effect at the concentration used (Figures S1D and S1E). We also confirmed that Fe availability had no influence on IRT1 localization (Figures S1F and S1G) (Barberon et al., 2011).

The transcriptional activation of *IRT1* gene expression by iron starvation responds to shoot-borne systemic signals. Split-root experiments, where only half of the root system is subjected to iron deficiency, indeed revealed the ability of plants to express *IRT1* in the iron-replete half of the root system (Vert et al.,

(D) Quantification of the co-localization between *irt1-1*/IRT1-mCit and endosomal markers from the same experiments as in (C). The center of mass of each particle was used to determine the percentage of coincidence. Error bars represent SD (n = 18). The asterisks indicate significant differences (Mann-Whitney, $p < 0.0001$).

(E) Time series of 35S::IRT1-mCit fluorescence upon various non-iron metal regimes. Scale bars, 100 μm.

(F) Western blot analyses on 35S::IRT1-mCit-expressing plants grown as in (E). Protein levels were detected using anti-GFP, and anti-tubulin antibodies to control for loading.

2003). To investigate the origin of signals underlying the retrieval of IRT1 from the cell surface upon non-iron metal excess, we carried out split-root approaches. These experiments showed that IRT1 accumulated in intracellular vesicles only in the half subjected to non-iron metal excess, while the other half remained unaffected, indicating that IRT1 is locally regulated by its secondary metal substrates (Figures S1H and S1I).

Non-iron Metals Change the Fate of IRT1 Protein

To evaluate the nature of the subcellular compartments associated with IRT1 upon changes in non-iron metal regimes, we co-localized IRT1-mCit with several endocytic markers. When plants were grown in the presence of physiological concentrations of non-iron metals, the intracellular pool of IRT1-mCit protein strongly co-localized with the EE marker Vha-a1 (Figures 1C and 1D). Consistently, very little overlap was observed between IRT1-mCit and the RabF2a LE marker. Two days of non-iron metal excess redistributed IRT1-mCit in the cell, with a decrease of the cell-surface and EE pools of IRT1 (Figures 1C and 1D). Consequently, IRT1-mCit was mostly found associated with LE, as visualized by the strong overlap with RabF2a. The removal of IRT1 from the cell surface and the shift in IRT1 localization to LE likely reflects a change into the degradative fate for IRT1.

The metal-dependent change in IRT1 localization initially observed after 2 days of metal excess occurred within hours of high metal level exposure. A short-term metal excess of only a few hours was indeed sufficient to deplete of IRT1 from the cell surface (Figure S1J, top). To confirm that IRT1 is targeted to the lytic vacuole for degradation upon metal excess, we took advantage of dark growth conditions that impair the vacuolar lytic activity and allow visualization of fluorescent proteins targeted to the vacuole (Tamura et al., 2003). Plants expressing IRT1-mCit grown under standard conditions showed weak vacuolar fluorescence after 4 hr of darkness, whereas plants concomitantly subjected to non-iron metal excess displayed enhanced fluorescence in the vacuole (Figures S1J–S1L). To better visualize the degradation of IRT1 upon non-iron metal stress, we sought to follow the accumulation of IRT1-mCit protein over time after transfer to non-iron metal excess. Since such metals compete with iron for uptake by IRT1, they indirectly interfere with iron homeostasis and modulate *IRT1* promoter activity (Figure S1M). To avoid incidental effect of non-iron metal nutrition on IRT1 levels, we used transgenic plants expressing the functional IRT1-mCit fusion driven by the constitutive CaMV35S promoter in wild-type plants. Non-iron metal excess led to a rapid internalization and degradation of constitutively expressed IRT1-mCit protein (Figures 1E, 1F, and S1N), with no change in *IRT1-mCit* mRNA (Figure S1O). Hence, the concentration of non-iron metal substrates of IRT1 regulates the distribution and the fate of the IRT1 transporter in the cell.

Non-iron Metal-Dependent K63 Polyubiquitin-Mediated Endocytosis of IRT1

The metal-dependent endocytosis and degradation of IRT1 led us to investigate the influence of non-iron metal nutrition on IRT1 ubiquitination. Immunoprecipitation (IP) of constitutively expressed IRT1-mCit from plants grown in standard conditions or subjected to a 2-hr-metal excess allowed enrichment in IRT1-mCit (Figure 2A). Immunoblotting (IB) of IRT1-mCit IP with P4D1 general anti-Ub antibodies revealed a high-molecular-weight smear that is typical of ubiquitinated proteins. However, the pool of ubiquitinated IRT1-mCit protein appeared more intense and larger after non-iron metal excess, indicating that metal stress increases the pool of ubiquitinated IRT1 (Figure 2A). The same pattern was also observed using plants expressing IRT1-mCit driven by the *IRT1* promoter (Figure S2A). Metal excess not only increased the pool of ubiquitinated IRT1 in the cell but also led to a qualitative change in the type of ubiquitination targeting IRT1. Indeed, probing IRT1-mCit IP with Apu3 antibodies, which recognize polyUb chains linked by residue K63 (Newton et al., 2008), revealed that IRT1 is decorated with K63-linked Ub chains upon metal stress (Figure 2B). These K63-linked chains have previously been associated with endocytosis in yeast, mammals, and more recently in plants (Huang et al., 2007; Lauwers et al., 2010; Martins et al., 2015).

To investigate deeper the role of ubiquitination in IRT1 endocytosis, we generated transgenic lines expressing the non-ubiquitinatable $IRT1_{2KR}$ mutant version (Barberon et al., 2011), carrying the K154R and K179R substitutions, fused to mCit and driven by the *IRT1* promoter in *irt1-1*. Expression of $IRT1_{2KR}$-mCit complemented the chlorosis and growth defects of *irt1-1*, indicating that it is fully functional (Figure S2B). $IRT1_{2KR}$-mCit protein was found exclusively at the PM upon standard conditions (Figure 2C), consistent with previous results (Barberon et al., 2011, 2014). Interestingly, $IRT1_{2KR}$-mCit failed to be endocytosed upon metal excess (Figures 2C and S2C), indicating that responses to non-iron metals require ubiquitination of residues K154 and K179. To decipher where ubiquitination acts on the endocytic trafficking of IRT1, plants expressing IRT1- or $IRT1_{2KR}$-mCit were treated with the fungal drug Brefeldin A (BFA), which creates in *Arabidopsis* roots an aggregation of internalized proteins in so-called BFA bodies (Geldner et al., 2003), in the absence of *de novo* protein synthesis. While wild-type IRT1-mCit largely accumulated in BFA bodies, $IRT1_{2KR}$-mCit appeared completely insensitive to BFA indicating that ubiquitination of residues K154 and K179 is essential for retrieving IRT1 from the cell surface (Figure S2D).

Taken together, these results clearly point to the importance of ubiquitination at the early stages of IRT1 endocytosis and to the crucial role of K63-linked Ub chains targeting residues K154 and K179 upon metal oversupply to regulate the distribution of IRT1 in the cell.

The IDF1 E3 Ligase Drives the Non-iron Metal-Dependent Endocytosis of IRT1

The ubiquitination of IRT1 requires the IDF1 RING E3 ligase (Shin et al., 2013), although the biological function of IDF1 has remained unclear since the ubiquitination of IRT1 was thought to be constitutive (Barberon et al., 2011). To evaluate the possible implication of IDF1 in root responses to non-iron metals, we first scored the root length of wild-type and *idf1-1* loss-of-function mutant plants on media containing physiological concentrations or an excess of non-iron metals. Wild-type plants showed slightly decreased root length when grown in the presence of non-iron metal excess (Figures 3A and 3B). In contrast, *idf1* showed increased sensitivity to metal stress, as attested by

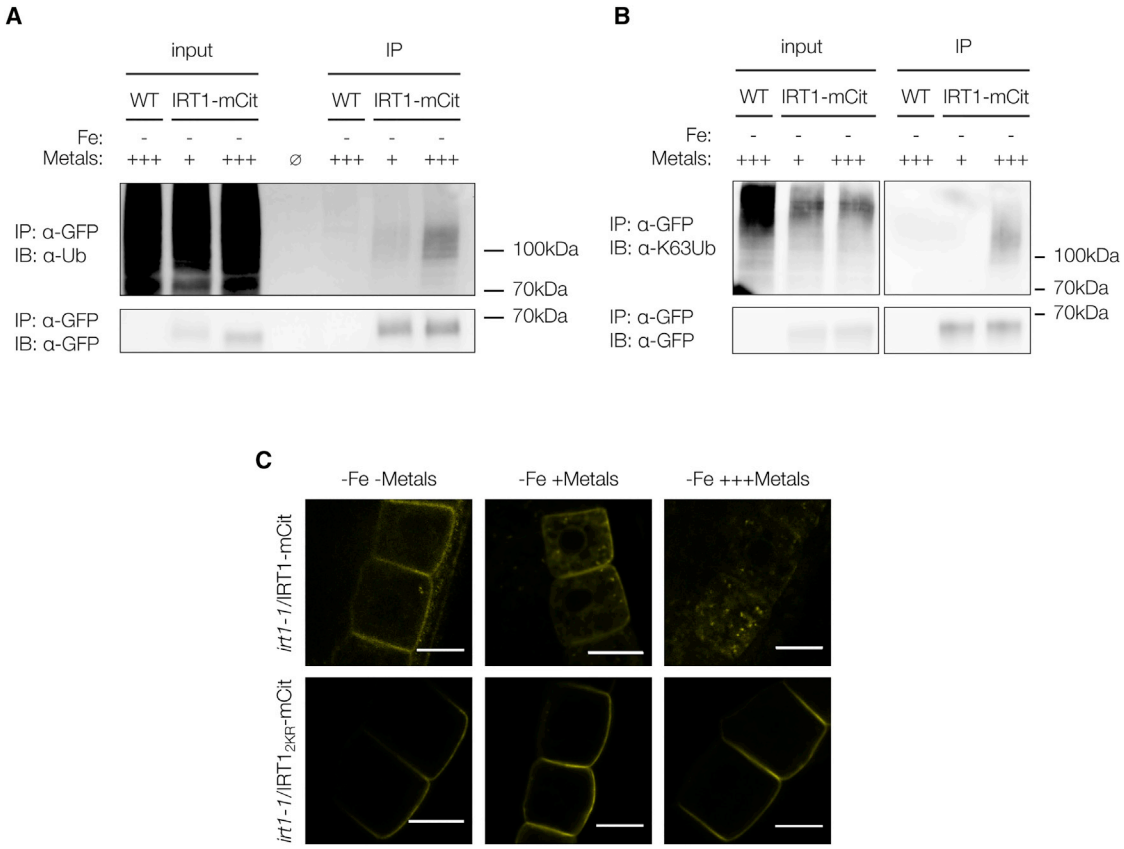

Figure 2. IRT1 Is Post-translationally Regulated by K63 Polyubiquitination in Response to Its Non-iron Metal Substrates

(A) *In vivo* ubiquitination analyses of IRT1 in response to non-iron metals. Immunoprecipitation (IP) was performed using anti-GFP antibodies on solubilized protein extracts from wild-type and 35S::IRT1-mCit plants and subjected to immunoblotting (IB) with anti-Ub (P4D1, top) and anti-GFP antibodies (bottom). Non-iron metal excess was applied for 2 hr.

(B) *In vivo* K63 polyubiquitination analyses of IRT1 in response to non-iron metals. IPs were probed with anti-K63 polyUb and anti-GFP antibodies. This blot is cropped from Figure 5F.

(C) Confocal microscopy analyses of *irt1-1*/IRT1-mCit and *irt1-1*/IRT1$_{2KR}$-mCit plants. Non-iron metal excess was applied for 2 hr. Scale bars, 10 μm.

the strong reduction in root length observed. The hypersensitivity of *idf1* to metal excess was accompanied with greater leaf content in Zn, Mn, and Co compared to wild-type (Figure S3A). Consistently, IRT1 protein accumulated at higher levels in *idf1* than in wild-type plants in response to non-iron metal excess, with no change in mRNA accumulation (Figures 3C and S3B). When expressed in the *idf1* mutant background, IRT1-mCit failed to be properly sorted for degradation in response to non-iron metals and was still found at the cell surface and in endosomes (Figures 3D and 3E). This was associated with a strong reduction of IRT1-mCit ubiquitination and more specifically K63 polyubiquitination in *idf1* upon non-iron metal stress (Figure 3F). Altogether, these observations clearly establish IDF1 as the E3 Ub ligase driving the metal-dependent K63 polyUb-mediated vacuolar targeting of IRT1.

Phosphorylation of IRT1 Is Required for IDF1-Dependent Destabilization

Phosphorylation often appears as a prerequisite for ubiquitination (Skaar et al., 2013). To better understand the mechanism by which non-iron metals trigger the recruitment of IDF1 and the K63 polyUb-dependent vacuolar targeting of IRT1, we therefore assessed whether IRT1 was phosphorylated in response to metals. We probed IRT1-mCit IP from plants grown under standard conditions, or subjected to a short-term metal excess, with anti-phosphothreonine antibodies. A smear was specifically observed for IRT1-mCit immunoprecipitates from plants challenged with an excess of non-iron metals (Figure 4A). Neither wild-type plants nor IRT1-mCit plants grown under standard non-iron metal conditions showed similar high molecular smear, indicating that the observed signal is specific of IRT1 and of metal excess. This laddering is reminiscent of what we observed for ubiquitinated forms of IRT1 and suggests that the K63 polyubiquitinated pool of IRT1 is also phosphorylated.

The *Arabidopsis* genome encodes over 900 kinases (Zulawski et al., 2014). Among the different families of plant kinases, the CIPK family has emerged as of critical importance for controlling the activity of transporters and channels (Ho et al., 2009; Ragel et al., 2015; Xu et al., 2006). We therefore directly tested for yeast two-hybrid interaction between the large cytosolic loop of IRT1

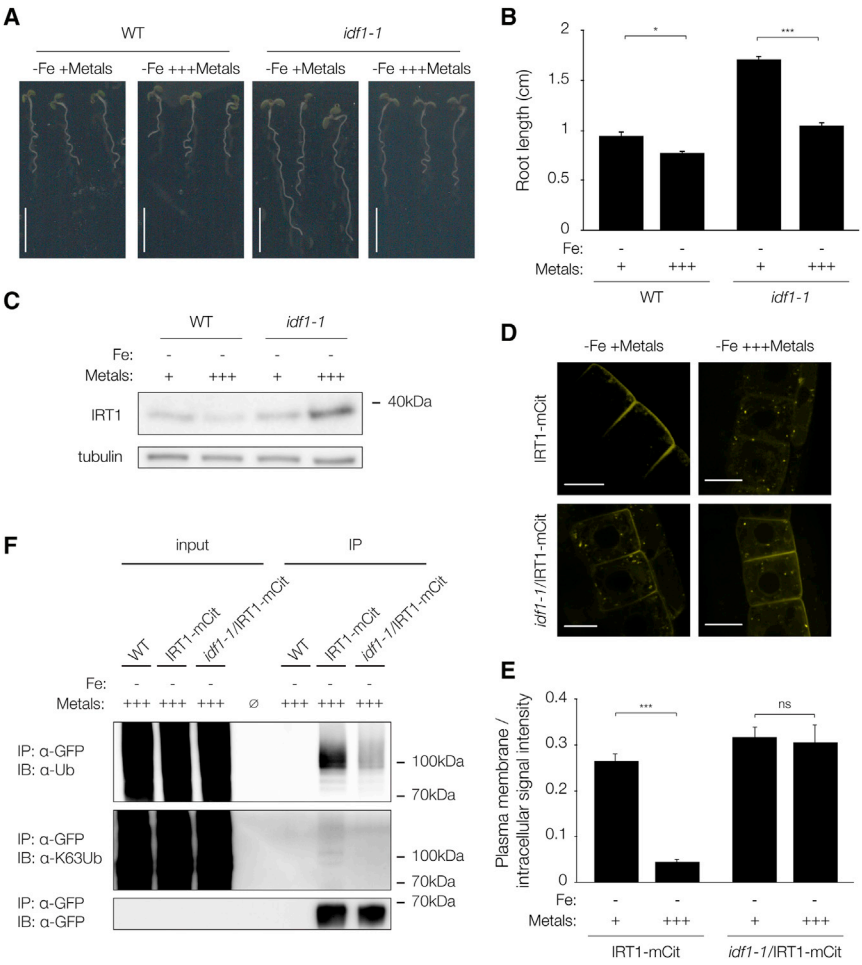

Figure 3. IDF1 Mediates IRT1 K63 Polyubiquitination in Response to Non-iron Metal Excess

(A) Phenotypic analyses of 7-day-old wild-type (WT) and *idf1-1* seedlings. Scale bars, 5 mm.

(B) Root length quantification of plants grown as in (A). Error bars represent SD (n = 40). The asterisks indicate significant differences (Mann-Whitney, $p < 0.0001$).

(C) Western blot analyses of plants cultivated as in (A). IRT1 protein levels were detected using anti-IRT1 antibodies. Anti-tubulin antibodies were used to control for loading.

(D) Confocal microscopy analyses of IRT1-mCit and *idf1-1*/IRT1-mCit plants. Non-iron metal excess was applied for 2 hr. Scale bars, 10 μm.

(E) Quantification of IRT1-mCit subcellular localization in IRT1-mCit and *idf1-1*/IRT1-mCit plants grown as in (D). Error bars represent SD (n = 15). The asterisks indicate significant difference (Mann-Whitney, $p < 0.0001$).

(F) *In vivo* ubiquitination analyses of IRT1. IP was performed using anti-GFP antibodies on solubilized protein extracts from wild-type (WT), IRT1-mCit, and *idf1-1*/IRT1-mCit plants and subjected to IB with anti-Ub (P4D1), anti-K63 polyUb (Apu3), and anti-GFP antibodies. Non-iron metal excess was applied for 2 hr.

(hereafter named IRT1c), which contains residues K154, K179, and the 26 *Arabidopsis* CIPKs. Only yeast co-expressing CIPK23 and IRT1c grew on selective medium (Figure S4A). The interaction between IRT1c and CIPK23 was also observed in the reverse orientation (Figure 4B). This interaction was confirmed by *in vitro* pull-down (PD) using recombinant IRT1c and CIPK23 proteins purified from *E. coli* (Figure S4B). The genetic contribution of CIPK23 was therefore evaluated in the context of plant responses to metal stress mediated by IRT1 destabilization. The *cipk23-5* knockout mutant showed dramatically reduced growth on medium containing high concentrations of metals (Figures 4C and 4D). This hypersensitivity to non-iron metals correlates with a strong accumulation of Zn, Mn, and Co in *cipk23-5*, compared to wild-type plants (Figure S4C). Furthermore, this was accompanied by a failure of *cipk23-5* mutant plants to target IRT1 protein to the vacuole upon non-iron metal excess (Figures 4E and 4F). This provides compelling genetic evidence for CIPK23 involvement in responses to non-iron metal excess.

CIPK-dependent phosphorylation of transporters and channels has been demonstrated to regulate ion transport activity per se (Ho et al., 2009; Li et al., 2006; Ragel et al., 2015; Xu et al., 2006). However, since loss of CIPK23 abolishes the non-iron metal-dependent endocytosis of IRT1 (Figures 4E and 4F), we speculated that CIPK23 controls the recruitment of IDF1 required for subsequent K63 polyUb-mediated endocytosis of IRT1. We took advantage of the ability of IRT1 and IDF1 to interact in split-Ub assays (Shin et al., 2013) to evaluate the role of CIPK23. CIPK23 expression in NubG-IRT1/IDF1-Cub-expressing yeast further increased the interaction between IRT1 and IDF1 (Figure 4G). The positive effect of CIPK23 on the IRT1/IDF1 interaction required CIPK23 kinase activity, as evidenced by the reduced and increased growth observed with kinase-dead and hyperactive CIPK23, respectively (Figure S4D). Bioinformatic prediction using the PhosPhAt 4.0 phosphorylation prediction software allowed us to identify putative phosphorylation sites in IRT1, including residue T175 located in close proximity to K154 and K179. The T175D phosphomimic mutation slightly enhanced the interaction between IRT1 and IDF1 in split-Ub assays (Figure S4E). Phosphomimic mutations of further neighboring phosphorylation sites (T148, S149, T152, S153, S183, and S184) strongly increased the interaction between IRT1 and IDF1 (Figure S4F). Consistently, CIPK23 was able to phosphorylate IRT1 *in vitro* and mutation of the putative phosphorylation sites in IRT1 abolished the CIPK23-mediated phosphorylation of IRT1 (Figure 4H). Taken together, these observations highlight the requirement for CIPK23-dependent phosphorylation of IRT1 to facilitate the recruitment of IDF1 in response to non-iron metal excess. Surprisingly, *cipk23* mutant showed increased accumulation of ubiquitinated forms of IRT1 (Figure 4I). The

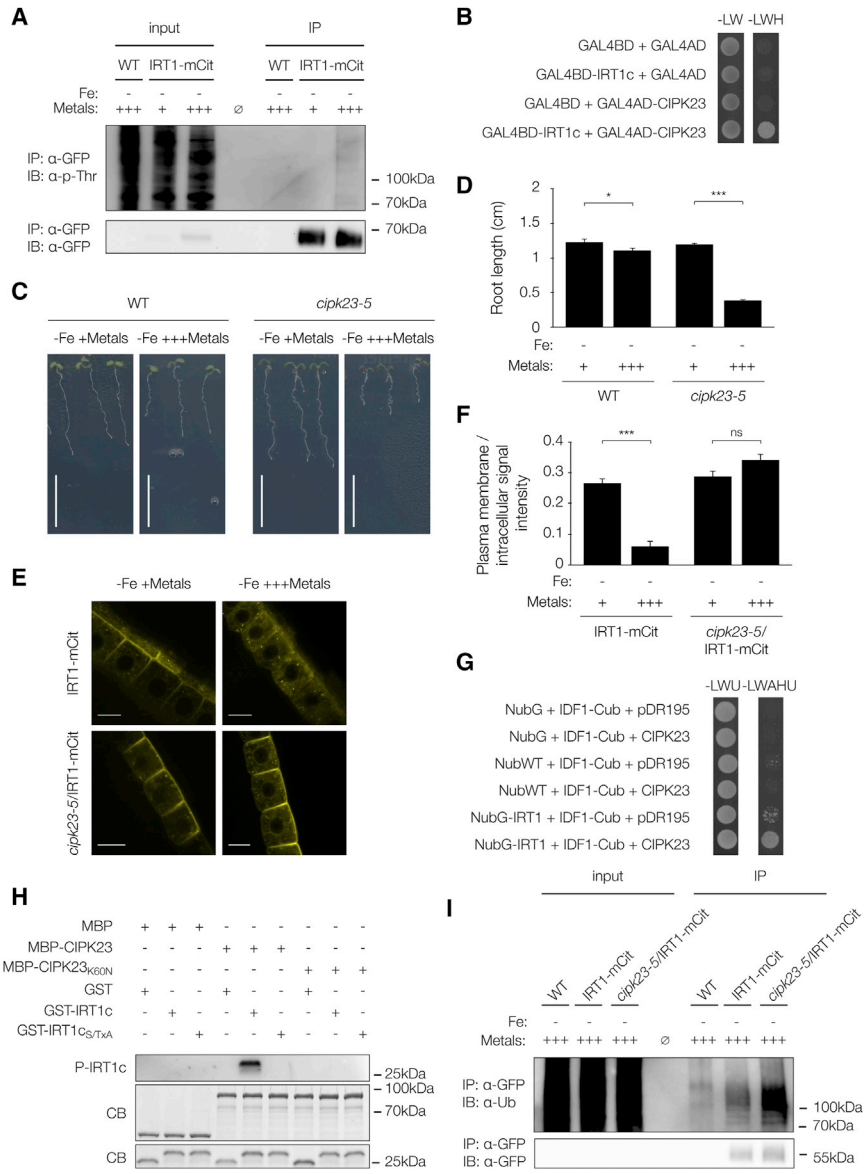

Figure 4. Phosphorylation of IRT1 by CIPK23 in Response to Metals Facilitates IDF1-Dependent Ubiquitination of IRT1

(A) *In vivo* phosphorylation analyses of IRT1 in response to non-iron-metals. IP was performed using anti-GFP antibodies on protein extracts from wild-type (WT) and 35S::IRT1-mCit plants and subjected to IB with anti-phospho-threonine and anti-GFP antibodies. Non-iron metal excess was applied for 2 hr.

(B) Yeast two-hybrid interaction between the cytosolic loop of IRT1 (IRT1c) and CIPK23.

(C) Phenotypic analyses of 7-day-old wild-type (WT) and *cipk23-5* seedlings. Scale bars, 5 mm.

(D) Root length quantification of plants grown as in (C). Error bars represent SD (n = 40). The asterisks indicate significant differences (Mann-Whitney, $p < 0.0001$).

(E) Confocal microscopy analyses of IRT1-mCit and *cipk23-5*/IRT1-mCit plants. Non-iron metal excess was applied for 2 hr. Scale bars, 10 μm.

(F) Quantification of IRT1-mCit subcellular localization in IRT1-mCit and *cipk23-5*/IRT1-mCit plants grown as in (E). Error bars represent SD (n = 15). The asterisks indicate significant difference (Mann-Whitney, $p < 0,0001$).

(G) Influence of CIPK23 on the interaction between IDF1 and IRT1. pDR195 and empty NubG were used as negative controls and NubWT as positive control.

(H) Kinase assay using recombinant IRT1c and CIPK23. Phosphorylation is detected using anti-phospho-T antibodies. GST, MBP, kinase-dead $CIPK23_{K60N}$ and $IRT1c_{S/TxA}$ carrying phospho-dead mutations were used as negative controls. CB, Coomassie blue staining.

(I) *In vivo* ubiquitination analyses of IRT1. IP was performed using anti-GFP antibodies on solubilized protein extracts from wild-type (WT), IRT1-mCit, and *cipk23-5*/IRT1-mCit plants and subjected to IB with anti-Ub (P4D1) and anti-GFP antibodies. Non-iron metal excess was applied for 2 hr.

inability of IRT1 to be targeted to the vacuole for degradation in *cipk23* likely prevents its deubiquitination in LE, explaining the accumulation of ubiquitinated IRT1. Taken together, these observations suggest that CIPK23 not only facilitates the recruitment of IDF1 to IRT1, but also directly impacts on IRT1 vacuolar targeting. This argues for a combined requirement of phosphorylation and K63 polyubiquitination for IRT1 to be properly sorted to the vacuole.

Histidine Residues in IRT1 Are Necessary for Direct Non-iron Metal Sensing

A stretch of histidine (H) residues (HGHGHGHG) is found in the large cytosolic loop of IRT1 between ubiquitination targets K154 and K179 and in close proximity to phosphorylation sites. Such H-rich motifs are found in several families of metal transporters from bacteria to mammals and have been postulated to serve as metal sensing domain (Eren et al., 2006). Using atomic absorption spectroscopy, we observed the presence of zinc on recombinant IRT1c purified from *E. coli* (Figure S5A). Zinc was however not detected on recombinant $IRT1c_{4HA}$, carrying substitution of the four H residues in alanine (A). Manganese was able to compete with zinc for binding to IRT1 (Figure S5A), consistent with the ability of IRT1 to bind manganese in electron paramagnetic resonance spectroscopy (Grossoehme et al., 2006). To investigate whether such H-rich stretch plays a role in metal sensing *in vivo* and in the metal-dependent degradation of IRT1, we generated a transgenic line expressing $IRT1_{4HA}$-mCit driven by *IRT1* promoter in *irt1-1*. In plants, expression of $IRT1_{4HA}$ restored the growth of the *irt1-1* loss-of-function mutant (Figure S5B), demonstrating that these H residues are not required for transport. Substitutions of these H residues however resulted in impaired ability

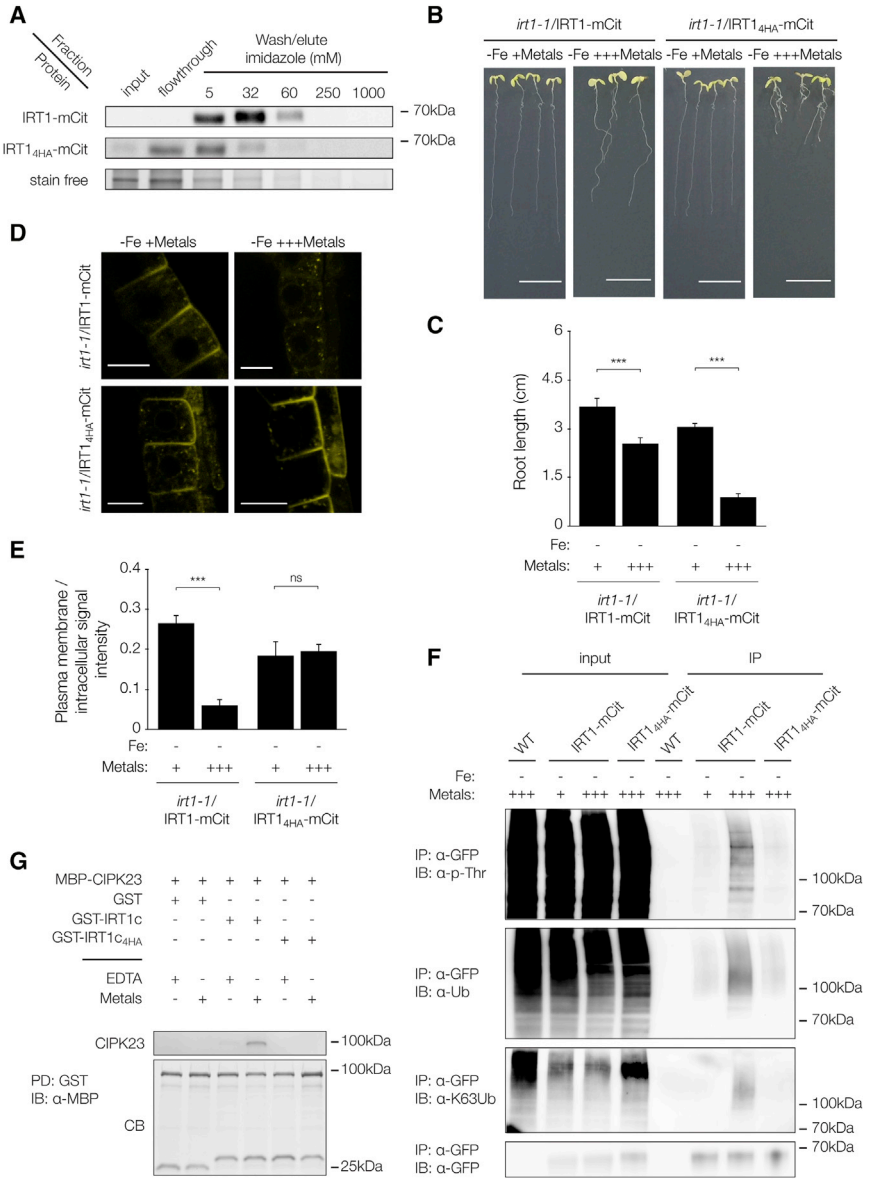

Figure 5. Direct Metal Binding to a Cytosolic Histidine-Stretch Drives IRT1 Responses to Metal Excess

(A) Metal binding analyses of IRT1 and IRT1$_{4HA}$. Protein extracts from 35S::IRT1-mCit and 35S::IRT1$_{4HA}$-mCit plants were subjected to immobilized metal (Co) ion affinity chromatography. Eluates were probed with anti-GFP antibodies. Stain free staining was used to illustrate the serial elutions with imidazole.

(B) Phenotypic analyses of 12-day-old *irt1-1*/IRT1-mCit and *irt1-1*/IRT1$_{4HA}$-mCit seedlings. Scale bars, 1 cm.

(C) Quantification of root length from plants grown as in (B). Error bars represent SD (n = 40). The asterisks indicate significant differences (Mann-Whitney, $p < 0.0001$).

(D) Confocal microscopy analyses of *irt1-1*/IRT1-mCit and *irt1-1*/IRT1$_{4HA}$-mCit. Non-iron metal excess was applied for 2 hr. Scale bars, 10 μm.

(E) Quantification of the ratio between PM and intracellular fluorescence signal intensities in plants grown as in (D). Error bars represent SD (n = 18). The asterisks indicate significant differences (Mann-Whitney, $p < 0.0001$).

(F) *In vivo* phosphorylation and ubiquitination analyses of IRT1 and IRT1$_{4HA}$ in response to non-iron metals. IP was performed using anti-GFP antibodies on protein extracts from wild-type (WT), 35S::IRT1-mCit, and 35S::IRT1$_{4HA}$-mCit plants and subjected to IB with anti-phospho-T, anti-Ub, anti-K63 polyUb, and anti-GFP antibodies. Non-iron metal excess was applied for 2 hr.

(G) Influence of metals on the direct *in vitro* interaction between IRT1c and CIPK23 recombinant proteins. GST and the metal binding-deficient IRT1c$_{4HA}$ were used as negative controls. PD, pull-down; CB, Coomassie blue staining.

of plant-expressed IRT1 to bind to a cobalt metal affinity resin (Figure 5A).

To genetically demonstrate the role of this H-rich stretch in responses to non-iron metal excess, we scored the root length of IRT1-mCit and IRT1$_{4HA}$-mCit lines on standard media or in non-iron metal excess conditions. IRT1$_{4HA}$-mCit-expressing plants were highly hypersensitive to non-iron metal excess, as visualized by the strong reduction in root length upon non-iron metal stress (Figures 5B and 5C). These plants also accumulated more non-iron metals than wild-type plants (Figure S5C), consistent with the severe growth reduction observed. Importantly, IRT1$_{4HA}$-mCit failed to relocalize from the PM and EE to the vacuole upon non-iron metal oversupply (Figures 5D and 5E), suggesting that the H residues found in IRT1 are involved in plant adjustment to non-iron metal availability. Consistent with IRT1 directly sensing non-iron metals in the cytosol, the IRT1$_{H104A}$ variant, deficient for metal transport (Rogers et al., 2000), did not respond to non-iron metal excess (Figures S5D and S5E). The inability of IRT1$_{4HA}$ to respond to metals is further corroborated by the lack of IRT1$_{4HA}$ phosphorylation, ubiquitination, and more specifically K63 polyubiquitination upon non-iron metal excess (Figure 5F). Interestingly, the interaction between IRT1 and CIPK23 in yeast required the presence of the H-rich stretch (Figure S5F), indicating that metal binding to IRT1 is likely required for CIPK23 recruitment and subsequent IDF1-dependent destabilization of IRT1. The metal dependence of the IRT1-CIPK23 interaction was further supported using recombinant proteins. Non-iron metals strongly enhanced the direct *in vitro* interaction between IRT1 and CIPK23 in pull-down assays (Figure 5G), indicating that CIPK23 is directly recruited to metal-loaded IRT1.

DISCUSSION

The processes by which multicellular organisms acquire extracellular nutrients is fairly well understood. However, the mechanisms

allowing the sensing, the signaling, and the integration of nutrient status have mostly been elusive. Within the context of essential transition metal homeostasis, we have now demonstrated that plants integrate several inputs underlying metal availability and unraveled the molecular framework for regulating plant metal uptake from the soil.

Plant roots frequently grow into patches of soil with contrasting nutrient level or availability and have evolved sophisticated developmental and physiological responses to maintain nutrient homeostasis. First, the plasticity of root development allows postembryonic densification of the root system in response to iron-rich areas to efficiently explore the bulk of the soil (Giehl et al., 2012). Second, plants have the amazing capacity to regulate nutrient uptake to sustain their needs, also taking into account soil heterogeneity. The transcriptional activation of *IRT1* is under the control of a shoot-borne signal, translating the shoot iron status, and root-derived signals underlying iron availability in the soil (Vert et al., 2002, 2003). Such intricate regulatory mechanisms ensure that iron-starved plants activate their high-affinity iron uptake system in soil patches that contain iron. Our work now establishes that an excess of secondary metal substrates of IRT1 locally regulate IRT1 at the post-translational level, by triggering IRT1 protein removal from the cell surface and promoting its vacuolar degradation. The plant root can therefore be seen as a mosaic of territories with different metal uptake capacities, aiming at optimizing iron uptake and limiting non-iron metal entry into plants.

Our findings shed light on the ability of IRT1 to act as a hybrid between a transporter and a receptor, also called transceptor, directly sensing its highly reactive non-iron metal substrates in the cytosol. H-rich stretches present in various metal transporter families across kingdoms were long proposed to serve as metal sensing domains (Eren et al., 2006). We now demonstrate using the IRT1 root metal transporter that such motif directly binds to non-iron metals to regulate root responses to metal availability. Interestingly, and in contrast to the CHL1/NRT1.1 plant transceptor (Ho et al., 2009; Vert and Chory, 2009), the signaling pathway initiated through the perception of non-iron metals by IRT1 targets IRT1 itself to regulate soil metal uptake. This short signaling pathway comprises the CIPK23 and IDF1 downstream players, which both post-translationally modify IRT1 to trigger its removal by K63 polyUb-mediated vacuolar targeting. This response is dependent on IRT1 transport activity and on the presence of the cytosol-exposed H-rich stretch, indicating that IRT1 senses non-iron metals in the cytoplasm. We propose a model that explains how plants integrate contrasting metal availability in soils (Figure 6). High non-iron metal influx, promoted by flooding or root growth through non-iron metal-rich soil patches for example, is locally perceived by non-iron metal loading of IRT1 H-stretch. Metal binding to these H residues likely folds the corresponding unstructured loop sitting at the permeation domain exit and allows CIPK23 recruitment. Interestingly, CIPK23 interacts with several PM transporters in the root epidermis and stands out as a central player in root responses to nutrient availability (Ho et al., 2009; Li et al., 2006; Ragel et al., 2015; Xu et al., 2006). The absence of crosstalk between reported CIPK23-dependent responses, as exemplified for potassium and nitrate by Ho et al. (2009), indicates that these processes are spatially restricted in root epidermal cells. A possible explanation may rely on the existence of different CIPK23-protein complexes, with elevated non-iron metals only activating the IRT1-containing CIPK23 pool. We have rather uncovered that CIPK23 is directly recruited to metal-loaded IRT1 upon excess of its secondary substrates, providing the molecular mechanism underlying the specificity of CIPK23-dependent phosphorylation. Upon non-iron metal excess, phosphorylation of IRT1 by CIPK23 creates a docking site for IDF1 and facilitates its recruitment. Although phosphorylation increases the IDF1/IRT1 interaction, IDF1 interacts weakly with IRT1 in the absence of CIPK23 (Shin et al., 2013). This is consistent with our observations that a small fraction of IRT1 is able to reach the vacuole under standard non-iron metal concentration (Barberon et al., 2011), where CIPK23 is not active, suggesting that a small fraction of IRT1 carries K63 polyUb chains. Upon metal stress, CIPK23-dependent phosphorylation of IRT1 boosts IDF1 recruitment and strongly increases the conversion of multimonoUb into K63 polyUb chains to target IRT1 to the vacuole. The IDF1-dependent extension of these monoUb into K63-linked polyUb chains likely occurs in endosomes and not at the cell surface. Genetic interference with non-iron metal response in *cipk23*, *idf1*, or in $IRT1_{4HA}$ backgrounds indeed results in PM and EE localization of IRT1 with failure to reach the vacuole (Figure S6), contrasting with the defective internalization observed for $IRT1_{2KR}$.

In addition to its role in recruiting IDF1, CIPK23 is also directly required for the trafficking of IRT1 to the vacuole. *cipk23* mutants show a vacuolar targeting defect while accumulating ubiquitinated forms of IRT1, pointing to the combined requirement for phosphorylation and K63 polyubiquitination to properly sort IRT1. K63 polyubiquitination is a well-established signal driving endosomal sorting of endocytic cargos. K63 polyUb chains increase the avidity of Ub-binding receptors from the ESCRT complex to ubiquitinated cargos, promoting their endosomal sorting (Hurley, 2008). The requirement for CIPK23 to deliver IRT1 in the vacuole suggests that IRT1 phosphorylation itself also participates in IRT1 recognition by subunits of the ESCRT complex. Alternatively, CIPK23 may phosphorylate and locally activate an ESCRT subunit during IRT1 endocytosis to ensure efficient and specific sorting of ubiquitinated IRT1. Phosphorylation of ESCRT components has indeed been previously associated with the regulation of their activity or their recruitment to endosomes (Morvan et al., 2012; Sun et al., 2016). Defective endosomal sorting associated with mutations in ESCRT subunits is notorious for triggering ubiquitinated protein accumulation in plants, due to impaired deubiquitination in LE (Isono et al., 2010; Kolb et al., 2015). Such inability of IRT1 to be properly sorted in *cipk23* certainly prevents deubiquitination in LE and yields accumulation of ubiquitinated IRT1, although IDF1 may be less efficiently recruited to IRT1 (Figure S6).

Our work nicely illustrates how CIPK23 and IDF1 are recruited to IRT1 by direct metal binding and by CIPK23-dependent phosphorylation, respectively. How these proteins are activated, however, remains unclear. Biochemical characterization of CIPK23 demonstrated that Mn^{2+} is the preferred cofactor

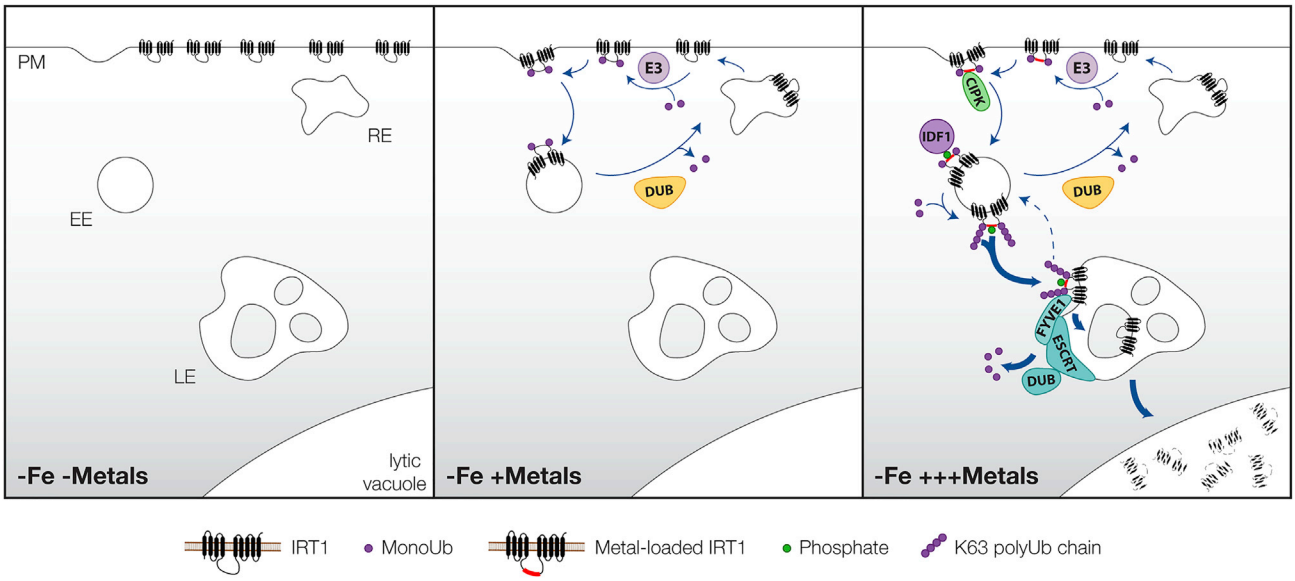

Figure 6. Model for the Non-iron Metal-Dependent Degradation of IRT1

In the combined absence of iron and non-iron metals, IRT1 protein accumulates at the cell surface and takes up iron in root epidermal cells (left). When iron is limited and non-iron metals found at physiological concentrations in soils, IRT1 is multi-monoubiquitinated at the cell surface by an unknown E3 Ub ligase (middle). This triggers IRT1 internalization toward EEs. Internalized IRT1 is likely deubiquitinated in EE by a deubiquitinase (DUB) to allow its recycling to the plasma membrane. When plants are iron-starved and facing elevated availability of non-iron metals in soils, the high influx rate of such metals is directly sensed by IRT1 through direct non-iron metal binding to histidine residues within the large cytosolic loop of IRT1. Metal-loaded IRT1 recruits the CIPK23 kinase that in turn phosphorylates S/T residues within the cytosolic loop of IRT1. CIPK23-dependent phosphorylation not only enhances the recruitment of the IDF1 E3 Ub ligase, which is itself activated by non-iron metal excess to further extends monoUb moieties into K63 polyUb chains but also directly impacts on the sorting of IRT1. As such, the decoration of IRT1 with both phosphate groups and K63 polyUb chains is necessary for its efficient sorting toward LEs and the vacuole for degradation. The dual regulation of IRT1 by its metal substrates, involving a systemic regulation by iron limitation and a local Ub-mediated degradation by non-iron metal excess, allows a fine spatiotemporal control of metal uptake. Plants protect themselves from the highly reactive nature and the high availability of non-iron metal substrates of IRT1 that can be encountered in soil patches by getting rid of IRT1, at the expense of iron uptake. PM, plasma membrane; EE, early endosome; RE, recycling endosome; LE, late endosome; DUB, deubiquitinase; ESCRT, endosomal sorting complex required for transport; CIPK, CIPK23.

over Mg^{2+}, leading to activation of its kinase activity (Hashimoto et al., 2012). CIPK23 may therefore be directly recruited to metal-bound IRT1 and loaded with Mn^{2+} to trigger IRT1 phosphorylation. The activity of IDF1 also appears to be controlled by metal binding to the H-stretch, as highlighted by the comparison of IRT1 ubiquitination profiles in genetic backgrounds affected in IRT1 vacuolar targeting. Whereas IRT1 ubiquitinated forms accumulate in *cipk23* as a result of basal IDF1 activity, plants unable to sense metals ($IRT1_{4HA}$) show a complete absence of IRT1 ubiquitination (Figure S6). Future work will therefore be necessary to unravel the precise mechanisms orchestrating the metal-dependent docking and activation of both CIPK23 and IDF1.

In summary, our findings shed light on the mechanism of non-iron metal sensing in plant roots and reveal a highly intricate network of regulations driving iron and metal absorption in plants. The ability of roots to separately monitor the availability of the different substrates from the major plant root metal transporter emerges as of central importance for the adaptation of roots to different soil environments. The precise control of IRT1 transceptor levels appears absolutely critical for proper iron and non-iron metal homeostasis in plants (Barberon et al., 2011, 2014; Vert et al., 2002). The molecular framework uncovered allowing IRT1 to perceive and to trigger its own degradation provides unique insight into the regulation of related ZIP metal transporters that are found from microorganisms to mammals.

STAR★METHODS

Detailed methods are provided in the online version of this paper and include the following:

- KEY RESOURCES TABLE
- CONTACT FOR REAGENT AND RESOURCE SHARING
- EXPERIMENTAL MODEL AND SUBJECT DETAILS
  - Plant Materials and Growth Conditions
  - Yeast strains and growth conditions
- METHOD DETAILS
  - Constructs and Transgenic Plants
  - Imaging
  - Elemental analyses
  - RNA extraction and real-time quantitative PCR
  - Western blot analysis and immunoprecipitation
  - Immobilized metal ion affinity chromatography
  - Constructs and *in vitro* pulldown assays
  - Metal detection on recombinant proteins
  - Yeast two-hybrid and Split-ubiquitin assays
  - Bioinformatics

- QUANTIFICATION AND STATISTICAL ANALYSIS
- DATA AND SOFTWARE AVAILABILITY

SUPPLEMENTAL INFORMATION

Supplemental Information includes six figures and one table and can be found with this article online at https://doi.org/10.1016/j.molcel.2018.02.009.

ACKNOWLEDGMENTS

We thank S. Merlot and S. Thomine for assistance with metal content analysis, J. Kudla for sharing published CIPK yeast two-hybrid vectors, F. Chaumont for split-Ub vectors, and F. Rubio for the *cipk23-5* mutant. We thank the Imagerie-Gif imaging facility, which is supported by the "Infrastructures en Biologie Santé et Agronomie" (IBiSA), the French National Research Agency (ANR-10-INSB-04-01), Saclay Plant Sciences initiative (ANR-10-LABX-0040-SPS), and the "Conseil Général de l'Essonne." G.D. is supported by a PhD fellowship from the Ministère de l'Education Nationale et de la Recherche. This work was supported by grants from CNRS (ATIP), Marie Curie Actions (PCIG-GA-2012-334021), and Agence Nationale de la Recherche (ANR-13-JSV2-0004-01) to G.V.

AUTHOR CONTRIBUTIONS

Conceptualization, G.D., J.N., E.Z., and G.V.; Methodology, G.D., J.N., and E.Z.; Validation, G.D., J.N., E.Z., and G.V.; Formal Analysis, G.D; Writing, G.D. and G.V.; Supervision, G.V.; Funding Acquisition, G.V.

DECLARATION OF INTERESTS

The authors declare no competing interests.

Received: August 23, 2017
Revised: December 22, 2017
Accepted: February 5, 2018
Published: March 15, 2018

REFERENCES

Barberon, M., Zelazny, E., Robert, S., Conéjéro, G., Curie, C., Friml, J., and Vert, G. (2011). Monoubiquitin-dependent endocytosis of the iron-regulated transporter 1 (IRT1) transporter controls iron uptake in plants. Proc. Natl. Acad. Sci. USA *108*, E450–E458.

Barberon, M., Dubeaux, G., Kolb, C., Isono, E., Zelazny, E., and Vert, G. (2014). Polarization of IRON-REGULATED TRANSPORTER 1 (IRT1) to the plant-soil interface plays crucial role in metal homeostasis. Proc. Natl. Acad. Sci. USA *111*, 8293–8298.

Belda-Palazon, B., Rodriguez, L., Fernandez, M.A., Castillo, M.C., Anderson, E.A., Gao, C., Gonzalez-Guzman, M., Peirats-Llobet, M., Zhao, Q., De Winne, N., et al. (2016). FYVE1/FREE1 interacts with the PYL4 ABA receptor and mediates its delivery to the vacuolar degradation pathway. Plant Cell. Published online: August 5, 2016. https://doi.org/10.1105/tpc.16.00178.

Besserer, A., Burnotte, E., Bienert, G.P., Chevalier, A.S., Errachid, A., Grefen, C., Blatt, M.R., and Chaumont, F. (2012). Selective regulation of maize plasma membrane aquaporin trafficking and activity by the SNARE SYP121. Plant Cell *24*, 3463–3481.

Bolte, S., and Cordelières, F.P. (2006). A guided tour into subcellular colocalization analysis in light microscopy. J. Microsc. *224*, 213–232.

Briat, J.F., Fobis-Loisy, I., Grignon, N., Lobréaux, S., Pascal, N., Savino, G., Thoiron, S., von Wiren, N., and Van Wuytswinkel, O. (1995). Cellular and molecular aspects of iron metabolism in plants. Biol. Cell *84*, 69–81.

Brumbarova, T., Bauer, P., and Ivanov, R. (2015). Molecular mechanisms governing Arabidopsis iron uptake. Trends Plant Sci. *20*, 124–133.

Chaves-Sanjuan, A., Sanchez-Barrena, M.J., Gonzalez-Rubio, J.M., Moreno, M., Ragel, P., Jimenez, M., Pardo, J.M., Martinez-Ripoll, M., Quintero, F.J., and Albert, A. (2014). Structural basis of the regulatory mechanism of the plant CIPK family of protein kinases controlling ion homeostasis and abiotic stress. Proc. Natl. Acad. Sci. USA *111*, E4532–E4541.

Dettmer, J., Hong-Hermesdorf, A., Stierhof, Y.D., and Schumacher, K. (2006). Vacuolar H+-ATPase activity is required for endocytic and secretory trafficking in Arabidopsis. Plant Cell *18*, 715–730.

Ebine, K., Okatani, Y., Uemura, T., Goh, T., Shoda, K., Niihama, M., Morita, M.T., Spitzer, C., Otegui, M.S., Nakano, A., and Ueda, T. (2008). A SNARE complex unique to seed plants is required for protein storage vacuole biogenesis and seed development of Arabidopsis thaliana. Plant Cell *20*, 3006–3021.

Eide, D., Broderius, M., Fett, J., and Guerinot, M.L. (1996). A novel iron-regulated metal transporter from plants identified by functional expression in yeast. Proc. Natl. Acad. Sci. USA *93*, 5624–5628.

Eren, E., Kennedy, D.C., Maroney, M.J., and Argüello, J.M. (2006). A novel regulatory metal binding domain is present in the C terminus of Arabidopsis Zn2+-ATPase HMA2. J. Biol. Chem. *281*, 33881–33891.

Gao, C., Luo, M., Zhao, Q., Yang, R., Cui, Y., Zeng, Y., Xia, J., and Jiang, L. (2014). A unique plant ESCRT component, FREE1, regulates multivesicular body protein sorting and plant growth. Curr. Biol. *24*, 2556–2563.

Geldner, N., Anders, N., Wolters, H., Keicher, J., Kornberger, W., Muller, P., Delbarre, A., Ueda, T., Nakano, A., and Jürgens, G. (2003). The Arabidopsis GNOM ARF-GEF mediates endosomal recycling, auxin transport, and auxin-dependent plant growth. Cell *112*, 219–230.

Geldner, N., Dénervaud-Tendon, V., Hyman, D.L., Mayer, U., Stierhof, Y.D., and Chory, J. (2009). Rapid, combinatorial analysis of membrane compartments in intact plants with a multicolor marker set. Plant J. *59*, 169–178.

Giehl, R.F., Lima, J.E., and von Wirén, N. (2012). Localized iron supply triggers lateral root elongation in Arabidopsis by altering the AUX1-mediated auxin distribution. Plant Cell *24*, 33–49.

Grossoehme, N.E., Akilesh, S., Guerinot, M.L., and Wilcox, D.E. (2006). Metal-binding thermodynamics of the histidine-rich sequence from the metal-transport protein IRT1 of Arabidopsis thaliana. Inorg. Chem. *45*, 8500–8508.

Hashimoto, K., Eckert, C., Anschütz, U., Scholz, M., Held, K., Waadt, R., Reyer, A., Hippler, M., Becker, D., and Kudla, J. (2012). Phosphorylation of calcineurin B-like (CBL) calcium sensor proteins by their CBL-interacting protein kinases (CIPKs) is required for full activity of CBL-CIPK complexes toward their target proteins. J. Biol. Chem. *287*, 7956–7968.

Ho, C.H., Lin, S.H., Hu, H.C., and Tsay, Y.F. (2009). CHL1 functions as a nitrate sensor in plants. Cell *138*, 1184–1194.

Huang, F., Goh, L.K., and Sorkin, A. (2007). EGF receptor ubiquitination is not necessary for its internalization. Proc. Natl. Acad. Sci. USA *104*, 16904–16909.

Hurley, J.H. (2008). ESCRT complexes and the biogenesis of multivesicular bodies. Curr. Opin. Cell Biol. *20*, 4–11.

Isono, E., Katsiarimpa, A., Müller, I.K., Anzenberger, F., Stierhof, Y.D., Geldner, N., Chory, J., and Schwechheimer, C. (2010). The deubiquitinating enzyme AMSH3 is required for intracellular trafficking and vacuole biogenesis in Arabidopsis thaliana. Plant Cell *22*, 1826–1837.

Ivanov, R., Brumbarova, T., Blum, A., Jantke, A.M., Fink-Straube, C., and Bauer, P. (2014). SORTING NEXIN1 is required for modulating the trafficking and stability of the Arabidopsis IRON-REGULATED TRANSPORTER1. Plant Cell *26*, 1294–1307.

James, P., Halladay, J., and Craig, E.A. (1996). Genomic libraries and a host strain designed for highly efficient two-hybrid selection in yeast. Genetics *144*, 1425–1436.

Kasai, K., Takano, J., Miwa, K., Toyoda, A., and Fujiwara, T. (2011). High boron-induced ubiquitination regulates vacuolar sorting of the BOR1 borate transporter in Arabidopsis thaliana. J. Biol. Chem. *286*, 6175–6183.

Kolb, C., Nagel, M.K., Kalinowska, K., Hagmann, J., Ichikawa, M., Anzenberger, F., Alkofer, A., Sato, M.H., Braun, P., and Isono, E. (2015). FYVE1 is essential for vacuole biogenesis and intracellular trafficking in Arabidopsis. Plant Physiol. *167*, 1361–1373.

Korshunova, Y.O., Eide, D., Clark, W.G., Guerinot, M.L., and Pakrasi, H.B. (1999). The IRT1 protein from Arabidopsis thaliana is a metal transporter with a broad substrate range. Plant Mol. Biol. *40*, 37–44.

Lauwers, E., Erpapazoglou, Z., Haguenauer-Tsapis, R., and André, B. (2010). The ubiquitin code of yeast permease trafficking. Trends Cell Biol. *20*, 196–204.

Li, L., Kim, B.G., Cheong, Y.H., Pandey, G.K., and Luan, S. (2006). A Ca(2)+ signaling pathway regulates a K(+) channel for low-K response in Arabidopsis. Proc. Natl. Acad. Sci. USA *103*, 12625–12630.

Livak, K.J., and Schmittgen, T.D. (2001). Analysis of relative gene expression data using real-time quantitative PCR and the 2(-Delta Delta C(T)) method. Methods *25*, 402–408.

Marquès-Bueno, M.D.M., Morao, A.K., Cayrel, A., Platre, M.P., Barberon, M., Caillieux, E., Colot, V., Jaillais, Y., Roudier, F., and Vert, G. (2016). A versatile Multisite Gateway-compatible promoter and transgenic line collection for cell type-specific functional genomics in Arabidopsis. Plant J. *85*, 320–333.

Martins, S., Dohmann, E.M., Cayrel, A., Johnson, A., Fischer, W., Pojer, F., Satiat-Jeunemaître, B., Jaillais, Y., Chory, J., Geldner, N., and Vert, G. (2015). Internalization and vacuolar targeting of the brassinosteroid hormone receptor BRI1 are regulated by ubiquitination. Nat. Commun. *6*, 6151.

Morvan, J., Rinaldi, B., and Friant, S. (2012). Pkh1/2-dependent phosphorylation of Vps27 regulates ESCRT-I recruitment to endosomes. Mol. Biol. Cell *23*, 4054–4064.

Murashige, T., and Skoog, F. (1962). A revised medium for rapid growth and bioassays with tobacco tissue cultures. Physiol. Plant. *15*, 473–497.

Newton, K., Matsumoto, M.L., Wertz, I.E., Kirkpatrick, D.S., Lill, J.R., Tan, J., Dugger, D., Gordon, N., Sidhu, S.S., Fellouse, F.A., et al. (2008). Ubiquitin chain editing revealed by polyubiquitin linkage-specific antibodies. Cell *134*, 668–678.

Ragel, P., Ródenas, R., García-Martín, E., Andrés, Z., Villalta, I., Nieves-Cordones, M., Rivero, R.M., Martínez, V., Pardo, J.M., Quintero, F.J., and Rubio, F. (2015). The CBL-Interacting Protein Kinase CIPK23 Regulates HAK5-Mediated High-Affinity K+ Uptake in Arabidopsis Roots. Plant Physiol. *169*, 2863–2873.

Rogers, E.E., Eide, D.J., and Guerinot, M.L. (2000). Altered selectivity in an Arabidopsis metal transporter. Proc. Natl. Acad. Sci. USA *97*, 12356–12360.

Séguéla, M., Briat, J.F., Vert, G., and Curie, C. (2008). Cytokinins negatively regulate the root iron uptake machinery in Arabidopsis through a growth-dependent pathway. Plant J. *55*, 289–300.

Shi, J., Kim, K.N., Ritz, O., Albrecht, V., Gupta, R., Harter, K., Luan, S., and Kudla, J. (1999). Novel protein kinases associated with calcineurin B-like calcium sensors in Arabidopsis. Plant Cell *11*, 2393–2405.

Shin, L.J., Lo, J.C., Chen, G.H., Callis, J., Fu, H., and Yeh, K.C. (2013). IRT1 degradation factor1, a ring E3 ubiquitin ligase, regulates the degradation of iron-regulated transporter1 in Arabidopsis. Plant Cell *25*, 3039–3051.

Skaar, J.R., Pagan, J.K., and Pagano, M. (2013). Mechanisms and function of substrate recruitment by F-box proteins. Nat. Rev. Mol. Cell Biol. *14*, 369–381.

Sun, S., Sun, L., Zhou, X., Wu, C., Wang, R., Lin, S.H., and Kuang, J. (2016). Phosphorylation-Dependent Activation of the ESCRT Function of ALIX in Cytokinetic Abscission and Retroviral Budding. Dev. Cell *37*, 581.

Tamura, K., Shimada, T., Ono, E., Tanaka, Y., Nagatani, A., Higashi, S.I., Watanabe, M., Nishimura, M., and Hara-Nishimura, I. (2003). Why green fluorescent fusion proteins have not been observed in the vacuoles of higher plants. Plant J. *35*, 545–555.

Vert, G., and Chory, J. (2009). A toggle switch in plant nitrate uptake. Cell *138*, 1064–1066.

Vert, G., and Chory, J. (2011). Crosstalk in cellular signaling: Background noise or the real thing? Dev. Cell *21*, 985–991.

Vert, G., Briat, J.F., and Curie, C. (2001). Arabidopsis IRT2 gene encodes a root-periphery iron transporter. Plant J. *26*, 181–189.

Vert, G., Grotz, N., Dédaldéchamp, F., Gaymard, F., Guerinot, M.L., Briat, J.F., and Curie, C. (2002). IRT1, an Arabidopsis transporter essential for iron uptake from the soil and for plant growth. Plant Cell *14*, 1223–1233.

Vert, G.A., Briat, J.F., and Curie, C. (2003). Dual regulation of the Arabidopsis high-affinity root iron uptake system by local and long-distance signals. Plant Physiol. *132*, 796–804.

Xu, J., Li, H.D., Chen, L.Q., Wang, Y., Liu, L.L., He, L., and Wu, W.H. (2006). A protein kinase, interacting with two calcineurin B-like proteins, regulates K+ transporter AKT1 in Arabidopsis. Cell *125*, 1347–1360.

Zulawski, M., Schulze, G., Braginets, R., Hartmann, S., and Schulze, W.X. (2014). The Arabidopsis Kinome: phylogeny and evolutionary insights into functional diversification. BMC Genomics *15*, 548.

STAR★METHODS

KEY RESOURCES TABLE

REAGENT or RESOURCE	SOURCE	IDENTIFIER
Antibodies		
Monoclonal anti-GFP HRP-coupled	Miltenyi Biotech	Cat# 130-091-833, RRID:AB_247003
Anti-Ub P4D1	Millipore	Cat# 05-944, RRID:AB_441944
Anti-K63 polyUb Apu3	Millipore	Cat# 05-1308, RRID:AB_1587580
Anti-Phospho-Thr	Cell Signaling Technology	Cat# 9381, RRID:AB_330301
Anti-IRT1	Séguéla et al., 2008	N/A
Anti-tubulin	Sigma-Aldrich	Cat# T5168, RRID:AB_477579
Anti-MBP	New England Biolabs	Cat# E8032S, RRID:AB_1559732
Bacterial and Virus Strains		
Rosetta2	Millipore	Cat # 71402
Chemicals, Peptides, and Recombinant Proteins		
BFA	Sigma-Aldrich	Cat# B6542
CHX	Sigma-Aldrich	Cat# C7698
Critical Commercial Assays		
μMACS GFP isolation kit	Miltenyi Biotec	Cat# 130-091-288
TALON Metal Affinity kit	Clontech	Cat# 635502
Glutathione agarose	Sigma	Cat# G4510
Amylose resin	New England Biolabs	Cat# E8021S
Deposited Data		
Mendeley data	This paper	https://doi.org/10.17632/m23brhzr4b.1
Experimental Models: Organisms/Strains		
Arabidopsis: *irt1-1*	Vert et al., 2002	N/A
Arabidopsis: *idf1-1*	Shin et al., 2013	SALK_038445
Arabidopsis: *cipk23-5*	Ragel et al., 2015	SALK_138057
Arabidopsis: VHAa1-RFP	Dettmer et al., 2006	N/A
Arabidopsis: RabF2a-mCherry	Geldner et al., 2009	NASC ID: N781672
Arabidopsis: mRFP-SYP22	Ebine et al., 2008	N/A
Arabidopsis: BOR4-GFP	Kasai et al., 2011	N/A
Arabidopsis: IRT1-mCit (and variants)	This paper	N/A
Yeast: AH109	James et al., 1996	N/A
Yeast: pJ69-4a	James et al., 1996	N/A
Yeast: THY.AP4	Besserer et al., 2012	N/A
Oligonucleotides		
Primers, See Table S1	This paper	N/A
Recombinant DNA		
pDONR211-mCit	Marquès-Bueno et al., 2016	N/A
pDONR221-IRT1-mCit (and variants)	This paper	N/A
p4p1r-prom35S	Marquès-Bueno et al., 2016	N/A
P4p1r-promIRT1	Marquès-Bueno et al., 2016	N/A
PG7m34GW-IRT1:: IRT1-mCit (and variants)	This paper	N/A
PG7m34GW-35S:: IRT1-mCit (and variants)	This paper	N/A
pGBT9.BS-CIPK1-26	Shi et al., 1999	N/A
pGAD.GH-IRT1c	This paper	N/A
pGADT7-CIPK23	This paper	N/A

(*Continued on next page*)

Continued

REAGENT or RESOURCE	SOURCE	IDENTIFIER
pGBKT7-IRT1c	Barberon et al., 2014	N/A
pNubG-IRT1 (and variants)	This paper	N/A
pCub-IDF1	This paper	N/A
pDR195-CIPK23 (and variants)	This paper	N/A
pGEX-6P-1-IRT1c (and variants)	This paper	N/A
pMalc2x-CIPK23 (and variants)	This paper	N/A
Software and Algorithms		
ImageJ plugin JACoP	Bolte and Cordelières, 2006	https://imagej.nih.gov/ij/plugins/track/jacop.html

CONTACT FOR REAGENT AND RESOURCE SHARING

Further information and requests for resources and reagents should be directed to and will be fulfilled by the Lead Contact, Grégory Vert (gregory.vert@i2bc.paris-saclay.fr).

EXPERIMENTAL MODEL AND SUBJECT DETAILS

Plant Materials and Growth Conditions

The *irt1-1*, *idf1-1*, *cipk23-5*, Vha-a1-RFP, RabF2a-mCherry, mRFP-SYP22 and BOR4-GFP *Arabidopsis* lines were described in previous studies (Dettmer et al., 2006; Ebine et al., 2008; Geldner et al., 2009; Kasai et al., 2011; Ragel et al., 2015; Shin et al., 2013; Vert et al., 2002). Wild-type plants and the various transgenic lines used in this study were grown in sterile conditions on vertical plates at 21°C with 16 hr light/8 hr dark cycles. To activate *IRT1* expression, wild-types, T-DNA-tagged mutants and the transgenic plants expressing IRT1 fusions under the control of *IRT1* promoter (*irt1-1*/IRT1::IRT1-mCit and variants) were grown under iron-deficient conditions. Transgenic plants constitutively expressing IRT1 fusions (35S::IRT1-mCit and variants) were also grown in the absence of iron for consistency. Non-iron metal excess conditions were carried out by adding a 10-fold concentration, using the half-strength Murashige and Skoog (MS) medium as reference (Murashige and Skoog, 1962). Such concentration of metals triggers a robust reduction in plant growth and is associated with increased metal accumulation in plant tissues.

For confocal microscopy analyses of transgenic plants using the *IRT1* promoter, iron starvation was performed by directly germinating seeds on half-strength MS lacking exogenous iron for 10 days. Plants were then transferred for 2 days in the same conditions (standard; -Fe +Metals) or in a medium containing ten times more Zn, Mn and Co (metal excess; -Fe +++ Metals). Non-iron metal deficiency was carried out by germinating seeds on medium lacking Fe, Zn, Mn and Co (deficiency; -Fe -Metals). Short-term non-iron metal treatments used a 2 hr transfer in liquid medium containing physiological (-Fe +Metals) or non-iron metal excess (-Fe +++Metals). Short-term Fe application was performed by challenging iron-starved IRT1-mCit (-Fe +Metals) for 2 hr with physiological Fe provision (50μM Fe-EDTA; +Fe +Metals) or with Fe excess (500μM Fe-EDTA; +++Fe +Metals). 35S::IRT1-mCitrine plants and corresponding mutated versions of IRT1 were imaged 7 days after germination, following a 2 hr transfer in physiological or non-iron metal excess conditions.

For biochemistry approaches, wild-type plants, *idf1-1*, and transgenic lines expressing IRT1-mCit and variants under the control of *IRT1* promoter were cultivated in iron-deficient conditions for 12 days before collecting samples. Constitutively-expressed IRT1-mCit lines were grown in iron-deficient conditions for 9 days (-Fe +Metals). Plants were then transferred for 2 hr in liquid medium lacking iron but containing either physiological levels of Zn, Mn and Co (-Fe +Metals) or a 10-fold increase of secondary substrates of IRT1 (-Fe +++Metals).

For split-root experiments, lateral root initiation was stimulated by cutting the primary root of 5-day-old-seedlings grown in iron-deficient conditions (-Fe + Metals) at the root-shoot junction. After 12 days, plants were transferred for 2 more days on plates containing one half with standard non-iron metal conditions, and one half subjected to a 10-fold metal excess (-Fe +++Metals).

For root growth analyses, plants were grown for 7 days in iron-deficient conditions and with either physiological level of non-iron metals (-Fe +Metals) or with a 10-fold excess of these metals (-Fe +++Metals). For transgenic lines expressing *IRT1-mCit* and variants under the control of *IRT1* promoter, root length was determined on 12-day-old plants for consistency with the timing of imaging by confocal microscopy. Aerial parts were then collected for elemental analyses. Roots were harvested for mRNA and protein extraction.

Yeast strains and growth conditions

For yeast two-hybrid experiments, the *Saccharomyces cerevisiae* AH109 and pJ69-4a yeast strains were used. For split-ubiquitin assays, the THY.AP4 strain was used. All strains were grown at 30°C in appropriate media for all experiments. Rich media (YPD with supplemental adenine) and synthetic drop-out (SD without selective amino acid) were used.

METHOD DETAILS

Constructs and Transgenic Plants

The *IRT1* open reading frame (ORF) was cloned into pDONR221 Gateway entry vector. The mutated IRT1-mCit versions ($IRT1_{2KR}$-mCit and $IRT1_{4HA}$-mCit) were generated by PCR. $IRT1_{2KR}$ contains lysine to arginine substitutions for residues K154 and K179. $IRT1_{4HA}$ contains histidine to alanine substitutions for residues H162, H164, H166 and H168. The mCitrine (mCit) coding sequence was cloned in loops of IRT1 by inserting BamHI restriction sites, yielding pDONR221-IRT1-mCit. Entry vectors carrying the *IRT1* and *35S* promoters (p4p1r-IRT1 and p4p1r-35S), and the mCit fluorescent protein (pDONR221-mCit) were previously described (Marquès-Bueno et al., 2016). Final destination vectors for expression in plants were obtained by using multisite Gateway recombination system (Life Technologies), using the pG7m34GW destination vector and the various pDONR221-IRT1-mCit entry clones to generate the IRT1::IRT1-mCit (or variants) and 35S::IRT1-mCit (or variants) constructs. Vectors carrying IRT1::IRT1-mCit and variants were transformed in *irt1-1* to assess functionality, *idf1-1*, *cipk23-5* or wild-type (Col-0) plants by the floral dipping technique using *Agrobacterium tumefaciens*, whereas 35S::IRT1-mCit were only transformed in wild-type plants (Col-0). For all constructs, around 20 independent T1 lines were isolated and three representative mono-insertion lines were selected in T2. Independent lines homozygous for the transgene were selected in T3. Primers used for construction and site-directed mutagenesis are listed in Table S1.

Imaging

Imaging was performed on inverted Leica SP2 and SP8X confocal microscopes. Within a given experiment, images from *irt1-1*/IRT1-mCit plants were taken using constant fluorescence to compensate for indirect effects of non-iron metals on *IRT1* transcription. For constitutively-expressed IRT1-mCit and variants, similar laser and detection settings were used for direct comparison of signal intensities and patterns between conditions and genotypes. For quantifications, z-stacks encompassing the whole cell volume were imaged on at least three different cells of three different plants during three independent experiments. The stacks were then subjected to maximum projection. The ratios of PM over intracellular relative signal content were obtained by selecting whole cell and intracellular content mean fluorescence with ImageJ. The fluorescence intensity in vacuoles was determined using identical regions of interest (ROI) for two different cells of three different plants during three independent experiments. Co-localization between IRT1-mCit and endosomal markers was performed on homozygous F3 plants resulting from the cross between *irt1-1*/IRT1-mCit and endosomal marker lines (Dettmer et al., 2006; Geldner et al., 2009). The Mander's overlap coefficient (MOC) and percentage of IRT1-mCit-positive endosomal structures showing overlap with Vha-a1-RFP or RabF2a-mCherry were determined using the center of mass of every particle with ImageJ plugin JACoP (Bolte and Cordelières, 2006). To ascertain that IRT1 is targeted to the vacuole upon non-iron metal excess, IRT1-mCit plants were crossed to plants expressing the tonoplast localized mRFP-SYP22 protein and F1 plants imaged.

CHX (Sigma-Aldrich) was applied to plants at a final concentration of 100 μM for 1 hr before treatment with 50μM BFA (Sigma-Aldrich) and maintained for the duration of BFA treatments. For dark treatment, plants were transferred to light or dark for 4 hr in liquid medium containing physiological level or excess of non-iron metals. All imaging experiments were performed in triplicates.

Elemental analyses

Leaves were harvested and rinsed for 5 min with deionized water before being dried at 65°C for 7 days. Tissues were digested completely in 2 mL of 70% (v/v) nitric acid in a DigiBlock ED36 (LabTech) at 80°C for 1 hr, 100°C for 1 hr, and 120°C for 2 hr. After dilution to 12 mL with ultrapure water, Mn, Zn and Co contents of the samples were determined by atomic absorption spectroscopy using an AA240FS flame spectrometer (Agilent Technologies). Metal content analyses were performed in triplicates.

RNA extraction and real-time quantitative PCR

Total RNA was extracted using QIAzol reagent following the manufacturer's instructions (QIAGEN). The integrity of RNA was verified by agarose gel electrophoresis, and an equal amount of total RNA (2 μg) was used for reverse transcription with anchored oligo (dT18) and RevertAid enzyme (ThermoFischer Scientific). For real-time PCR analyses, *IRT1-mCit*, *IRT1*, or *EF1α* were amplified with a Light-cycler 96 with SYBR Green I Master (Roche), using the primers described in Table S1. Experiments were done using three technical and three biological replicates. Relative expression of *IRT1-mCit* and *IRT1* was quantified with the $2^{-\Delta\Delta Ct}$ method (Livak and Schmittgen, 2001) using *EF1α* as a reference gene.

Western blot analysis and immunoprecipitation

For western blot analyses, total proteins were extracted from 100 mg of roots. For protein detection, the following antibodies were used: Monoclonal anti-GFP horseradish peroxidase-coupled (Miltenyi Biotec 130-091-833, 1/5,000), anti-Ub P4D1 (Millipore 05-944, 1/2,500), anti-K63 polyUb Apu3 (Millipore 05-1,308, 1/2,000), anti-phospho-threonine (Cell Signaling Technology 9381, 1/1,000), anti-IRT1 (Séguéla et al., 2008), and anti-tubulin (Sigma T5168, 1/5,000). Detection of HRP chemiluminescence was done on a ChemiDoc Touch (BioRad) with the help of SuperSignal West Dura Extended Duration Substrate (ThermoScientific).

IP experiments were performed using approximately 2 g of roots. Tissues were ground in liquid nitrogen and resuspended in RIPA buffer as previously described (Barberon et al., 2011). Samples were then centrifuged for 10 min at 5,000 g at 4°C. Total proteins contained in the supernatant were placed for 1 hr at 4°C on a rotating wheel to solubilize membrane proteins. Non-resuspended material was then pelleted for 45 min at 100,000 g at 4°C. IP were carried out using the μMACS GFP isolation kit (Miltenyi Biotec) and washes performed with the stringent RIPA buffer. IP and western blot analyses were performed in triplicates.

Immobilized metal ion affinity chromatography

The metal-binding capacity of IRT1-mCit and its $IRT1_{4HA}$-mCit was analyzed using TALON Metal Affinity Resin, according to the manufacturer's instructions (Clontech). Samples were prepared as described above for IP experiments before addition of 100 μL of TALON resin and incubation for 1 hr at 4°C on a rotating wheel. After centrifugation at 1,000 rpm, 100μL of the supernatant was collected as the flow through fraction. Three washes were performed with 200 μL of RIPA buffer supplemented with 5mM imidazole. Unbound and bound proteins were serially washed out and collected in each fraction by applying 200 μL of RIPA buffer containing 5, 32, 60, 250, or 1,000 mM imidazole. 20 μL of each fraction was subjected to SDS-PAGE. Metal binding experiments were done in triplicates.

Constructs and *in vitro* pulldown assays

For the production of recombinant proteins, wild-type and kinase-dead CIPK23 were cloned into pMALc2x using *Pst*I and *Hind*III. IRT1c and variants were cloned into pGEX-6P-1 at *BamH*I and *EcoR*I sites. Recombinant proteins were extracted from Rosetta2 cells expressing MBP, GST, MBP-CIPK23, GST-IRT1c, and variants for CIPK23 and IRT1c according to the manufacturer's recommendation. For pulldown experiments, 1μg of the respective proteins was incubated in binding buffer (50 mM Tris-HCl pH 6.7, 100 mM NaCl, 0.05% Tween-20, 1 mM Pefabloc) for 30 min at 4°C. Pulldown was performed using glutathione-agarose beads. MBP was detected using anti-MBP antibodies (New England Biolabs). To evaluate the effect of metals on the IRT1-CIPK23 interaction, recombinant GST-IRT1c and variants were incubated with 4 mM of non-iron metal substrates prior to pulldown.

Metal detection on recombinant proteins

Proteins were pulled down with glutathione-agarose beads, washed with TN buffer (20 mM Tris-HCl pH 7.5, 200 mM NaCl) and eluted with reduced glutathione. Eluates were dialyzed against TN buffer to eliminate glutathione. Zinc (500 nmoles), as a representative of non-iron metals, was added to recombinant GST, GST-IRT1c and GST-$IRT1c_{4HA}$ (40 nmoles) for 30 min and dialyzed overnight against TN to get rid of unbound zinc. Competition experiments were carried out in the presence of equimolar amounts of zinc and manganese, and zinc binding to recombinant proteins was determined. Samples were mineralized in nitric acid and subjected to atomic absorption spectroscopy using an AA240FS flame spectrometer (Agilent Technologies). Metal detection on recombinant proteins was performed in triplicates. Background zinc binding to GST was subtracted to GST-IRT1c and GST-$IRT1c_{4HA}$.

Yeast two-hybrid and Split-ubiquitin assays

For yeast two-hybrid assays, CIPKs were cloned in pGBT9.BS (GAL4BD-CIPK1-26) (Shi et al., 1999) and used with the cytosolic fragment of IRT1 cloned in pGAD.GH (GAL4AD-IRT1c). Interactions were also tested in reverse orientation, using pGBKT7-IRT1c (GAL4BD-IRT1c) and variants and pGADT7-CIPK23 (GAL4AD-CIPK23). Bait and prey vectors carrying CIPKs and IRT1c were transformed into AH109 or pJ69-4a yeast cells. Interactions were monitored on SD lacking selective amino acids. Interaction tests were performed in triplicates. For split-Ub assay, *IRT1* and $IRT1_{T175A}$, $IRT1_{T175D}$, $IRT1_{S/TxA}$, $IRT1_{S/TxD}$ variants were inserted into pNubG vector and the *IDF1* ORF cloned into pCub vector containing the PLV transcription factor (Besserer et al., 2012). $IRT1_{S/TxA}$, $IRT1_{S/TxD}$ were produced by gene synthesis and carry substitutions into alanine and aspartic acid, respectively, at sites T148, S149, T152, S153, T175, S183 and S184. The wild-type *CIPK23* coding sequence, the K60N kinase-dead or the T190D hyperactive CIPK23 mutants (Chaves-Sanjuan et al., 2014; Li et al., 2006) were inserted into the yeast expression vector pDR195. The wild-type Ub N-terminal fragment (NubWT) was used as a positive control and NubG as a negative control. Transformed THY.AP4 cells were selected on SD medium lacking leucine and tryptophan (SD-LW). NubG-IRT1/Cub-IDF1-expressing yeast were further transformed with pDR195 or pDR195-CIPK23 (and variants) and selected on selective medium lacking leucine, tryptophan, and uracil (SD-LWU). Protein-protein interaction was assessed by following the growth of transformed cells on selective medium lacking leucine, tryptophan, adenine, histidine and uracil (SD-LWAHU). Interaction tests were performed in triplicates.

The primers used in this study are described in Table S1.

Bioinformatics

Prediction of phosphorylation sites in IRT1 was achieved using the PhophAt 4.0 interface (phosphat.uni-hohenheim.de/phosphat.html). Results were filtered, focusing on predicted sites with the highest scores and targeting cytosolic loops. Using these criteria, we identified threonine T175 located in the large cytosolic loop between TM4 and TM5 and in close proximity with residues K154 and K179 as a good candidate.

QUANTIFICATION AND STATISTICAL ANALYSIS

All experiments were performed in triplicates. For confocal microscope experiments and biochemistry, a representative image is shown. Statistical analyses were performed using the software GraphPad Prism and the sample size and statistical tests used mentioned in the legend to figures.

DATA AND SOFTWARE AVAILABILITY

All images and blots have been deposited to Mendeley Data and are available at https://doi.org/10.17632/m23brhzr4b.1

Molecular Cell, Volume *69*

Supplemental Information

Metal Sensing by the IRT1 Transporter-Receptor Orchestrates Its Own Degradation and Plant Metal Nutrition

Guillaume Dubeaux, Julie Neveu, Enric Zelazny, and Grégory Vert

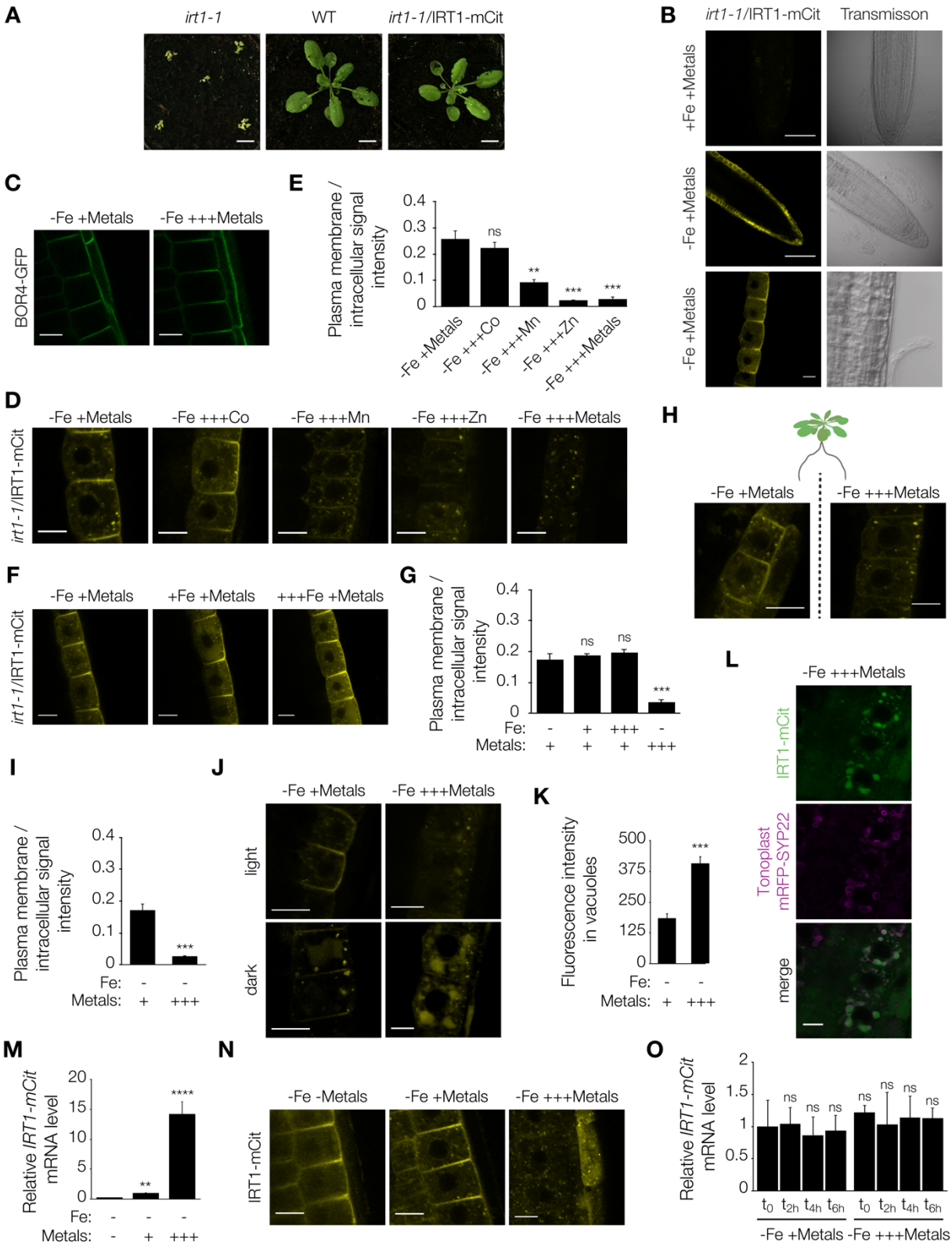

Figure S1. Detailed analysis of IRT1-mCit trafficking upon non-iron metal excess. Related to Figure 1.

(A) Phenotypic analyses of wild-type (WT), *irt1-1* and the *irt1-1*/IRT1::IRT1-mCit plants expressing a functional IRT1-mCit fusion protein. Scale bars=1cm. **(B)** Confocal microscopy analyses of root tip from *irt1-1*/IRT1-mCit plants grown for 12 days in iron-sufficient or iron-

deficient media, with physiological concentrations of non-iron metals. Scale bars=100µm (top and center), 10µm (bottom). **(C)** Confocal microscopy analyses of root epidermal cells from 35S::BOR4-GFP plants. Non-iron metal excess was applied for 2 days. **(D)** Subcellular localization of *irt1-1*/IRT1-mCit in response to excess of secondary metal substrates applied independently. **(E)** Ratio between PM and intracellular fluorescence signal intensities of *irt1-1*/IRT1-mCit from experiments performed as in (D). Error bars represent s.d. (n=18). The asterisks indicate significant differences to the -Fe +Metals control (One-Way ANOVA, Dunnett post-test, P<0.0001). **(F)** Subcellular localization of *irt1-1*/IRT1-mCit in response to iron availability in the growth medium. Plants were grown on media lacking iron and containing physiological concentrations of non-iron metals (-Fe +Metals), and subjected to either physiological iron provision (+Fe +Metals) or to a tenfold excess in iron (+++Fe +Metals) for 4 hours. (**G**) Ratio of *irt1-1*/IRT1-mCit plasma membrane (PM) to intracellular signal intensities from experiments performed as in (F). The -Fe +++Metal condition is used as positive control. Experiments were carried out in triplicates on stacks encompassing epidermal cells. Error bars represent standard deviation (s.d. ; n=18). The asterisks indicate significant differences to the –Fe +Metal condition (Mann-Whitney, P<0.0001). **(H)** Split-root experiments of *irt1-1*/IRT1-mCit plants transferred for 2 days to a plate with one half containing physiological concentrations of non-iron metals (-Fe +Metals) and one half containing non-iron metal excess (-Fe +++Metals). **(I)** Quantification of signal intensities of split-root-grown *irt1-1*/IRT1-mCit plants as in (H). Error bars represent s.d. (n=18). The asterisks indicate significant differences (Mann-Whitney, P<0.0001). **(J)** Vacuolar targeting of IRT1 in response to non-iron metal nutrition. Light grown *irt1-1*/IRT1-mCit seedlings were incubated in light or dark conditions for 4 hours in physiological concentration of non-iron metals (-Fe +Metals) or non-iron metal excess (-Fe +++Metals). **(K)** Quantification of *irt1-1*/IRT1-mCit vacuolar targeting in response to non-iron metals using plants grown as in (J). Error bars represent s.d. (n=18). The asterisks indicate significant differences (Mann-Whitney, P<0.0001). **(L)** Vacuolar targeting of IRT1 in response to non-iron metal excess in plants co-expressing IRT1-mCit and the tonoplast marker mRFP-SYP22. Plants were incubated in dark conditions and challenged with non-iron metals for 4 hours. Scale bars=10µm. **(M)** *IRT1-mCit* mRNA accumulation in 12-day-old *irt1-1*/IRT1-mCitrine plants. Non-iron metal excess was applied for 2 days. Error bars represent s.d. (n=3). The asterisks indicate significant differences (Kruskal-Wallis, **, P<0.001 ; ****, P<0.00001). **(N)** Confocal microscopy analyses of 35S::IRT1-mCit plants. Non-iron metal excess was applied for 2 hours. Scale bars=10µm. **(O)** *IRT1-mCit* mRNA accumulation in 35S::IRT1-mCit plants grown in conditions described in Figure 1E, 1F. Error bars represent s.d. (n=3). No statistical difference to the t_0 -Fe +Metals control were observed (Kruskal-Wallis, P>0.05).

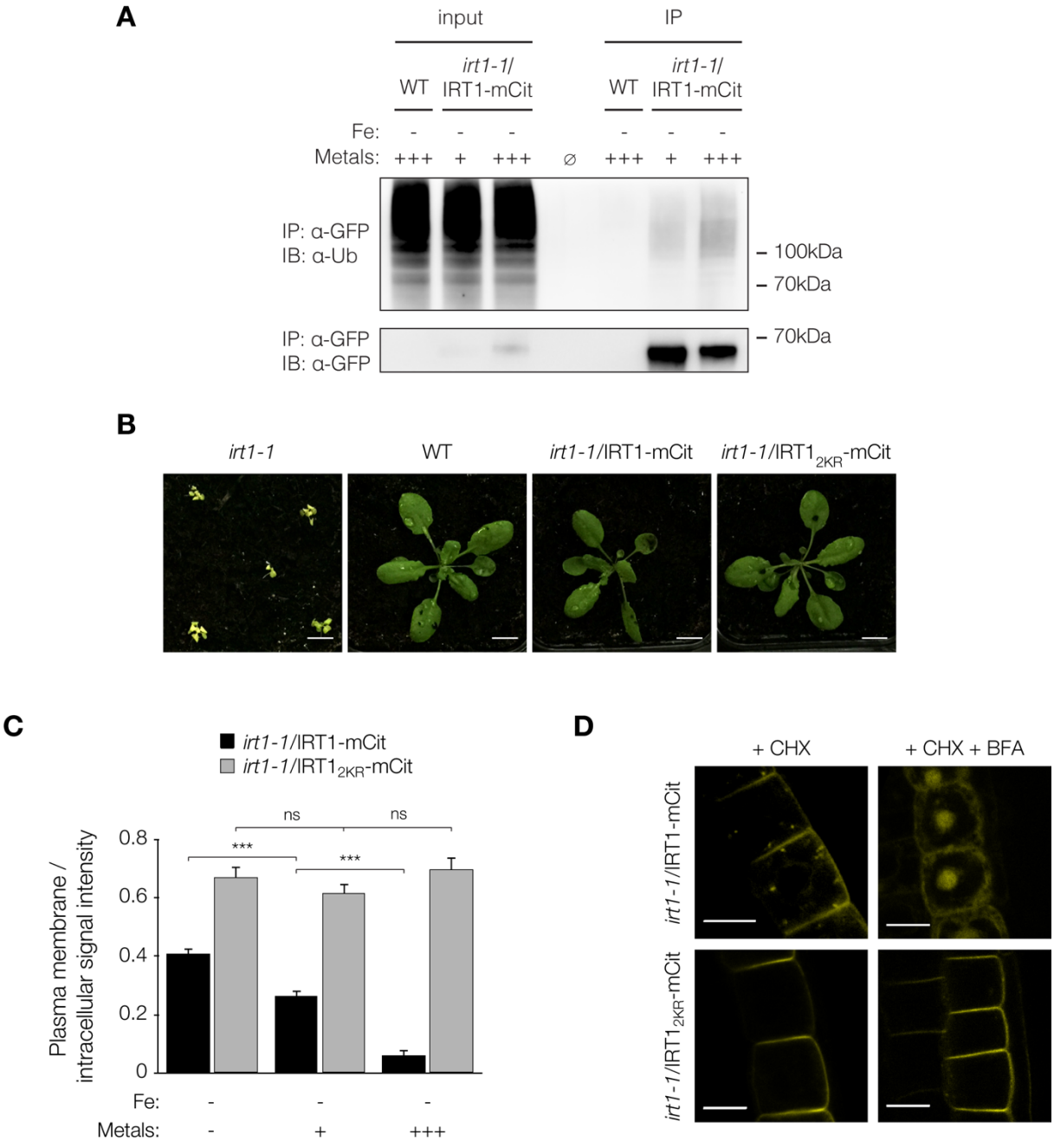

Figure S2. Non-iron metal substrates of IRT1 regulate its ubiquitination. Related to Figure 2.

(A) *In vivo* ubiquitination analyses of IRT1 in response to various non-iron metal regimes. Immunoprecipitation was performed using anti-GFP antibodies on solubilized protein extracts from wild-type and *irt1-1*/IRT1-mCit plants and subjected to immunoblotting with anti-Ub P4D1 (top) and anti-GFP (bottom). IB, immunoblotting ; IP, immunoprecipitation. Non-iron metal excess was applied for 2 hours. **(B)** Phenotypic analyses of wild-type (WT), *irt1-1*, *irt1-1*/IRT1-mCit and *irt1*/IRT1$_{2KR}$-mCit. Scale bars=1cm. **(C)** Ratio between PM and intracellular fluorescence signal intensities from experiments performed as in Figure 2C. Error bars represent s.d. (n=18). The asterisks indicate significant differences (Mann-Whitney, P<0.0001). **(D)** Sensitivity of *irt1-1*/IRT1-mCit and *irt1-1*/IRT1$_{2KR}$-mCit plants to BrefelfinA (BFA). Plants were pretreated with 100 µM cycloheximide (CHX) for 1 h and exposed to 100 µM CHX and 50 µM BFA for 3 hours. Scale bars=10µm.

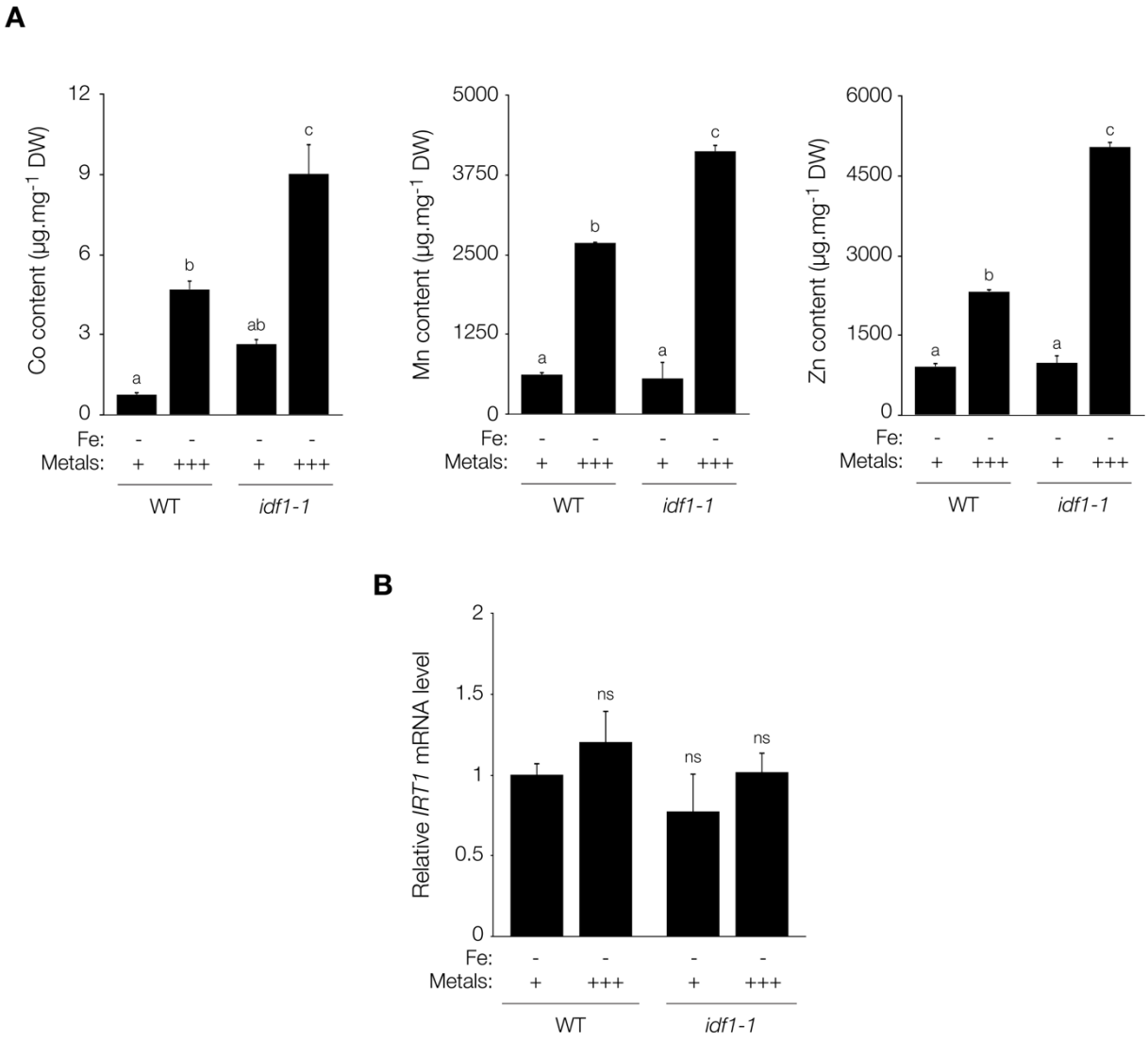

Figure S3. Metal content and molecular characterization of the *idf1-1* loss-of-function mutant. Related to Figure 3.

(A) Metal content analyses by atomic absorption spectrometry of 7-day-old wild-type and *idf1-1* seedlings described in Figure 3A. Experiments were carried out in triplicates. Error bars represent s.d. (n=3). Different letters indicate means that were statistically different by Tukey's multiple testing method ($P<0.05$). **(B)** *IRT1* mRNA accumulation from plants described in Figure 3A. No statistical difference –Fe +Metals condition for WT were observed (Kruskal-Wallis, $P>0.05$).

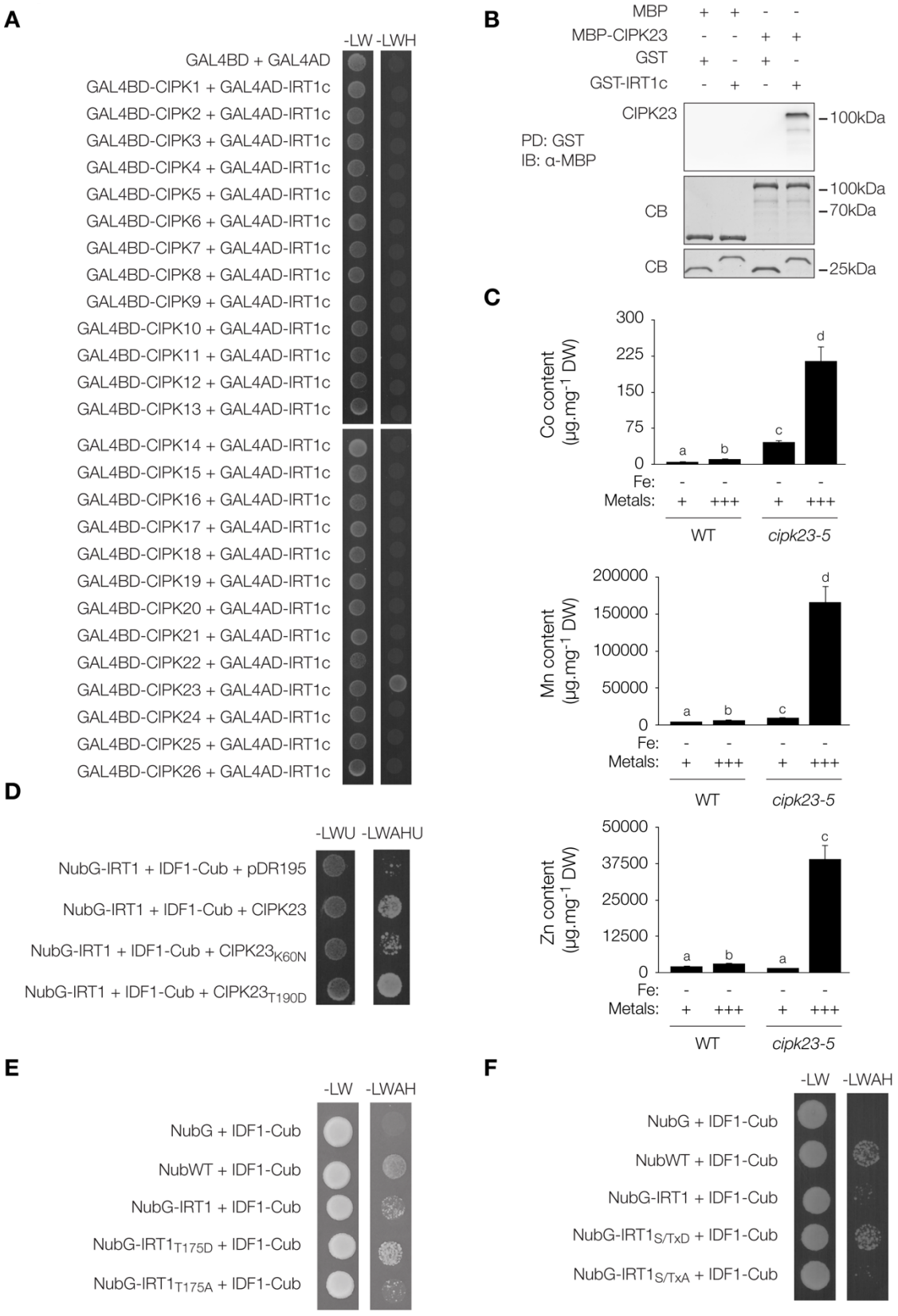

Figure S4. Phosphorylation of IRT1 by CIPK23 in response to metals mediates IDF1-dependent ubiquitination of IRT1. Related to Figure 4.

(A) Yeast two-hybrid interaction between the cytosolic loop of IRT1 (IRT1c) and the 26 CIPK family members from Arabidopsis. Empty bait and prey vectors were used as negative controls. Yeast were spotted on selective (SD-LWH) or non-selective (SD-LW) media. Experiments

were done in triplicates. **(B)** *In vitro* pulldown assay monitoring the interaction between IRT1 and CIPK23. GST and MBP alone are used as negative controls. PD, pulldown ; CB, coomassie blue staining. **(C)** Metal content analyses by atomic absorption spectrometry of 7-day-old wild-type and *cipk23-5* seedlings described in Figure 4C. Experiments were carried out in triplicates. Error bars represent s.d. (n=3). Different letters indicate means that were statistically different by Tukey's multiple testing method ($P<0.05$). **(D)** Split-Ub interaction between IRT1 and IDF1 in the presence of kinase-dead (K60N) and hyperactive (T190D) CIPK23. NubG and NubWT were used as negative and positive controls, respectively. Yeast were spotted on selective (SD-LWAHU) or non-selective (SD-LWU) media. Experiments were done in triplicates. **(E)** Split-ubiquitin interaction between IDF1 and IRT1 variants for threonine residue T175 (phosphomimic T175D and non-phosphorylatable T175A). NubG and NubWT were used as negative and positive controls, respectively. Yeast were spotted on selective (SD-LWAH) or non-selective (SD-LW) media. Experiments were done in triplicates. **(F)** Split-ubiquitin interaction between IDF1 and IRT1 variants for putative phosphorylation sites (phosphomimic S/TxD and non-phosphorylatable S/TxA). NubG and NubWT were used as negative and positive controls, respectively. Yeast were spotted on selective (SD-LWAH) or non-selective (SD-LW) media. Experiments were done in triplicates.

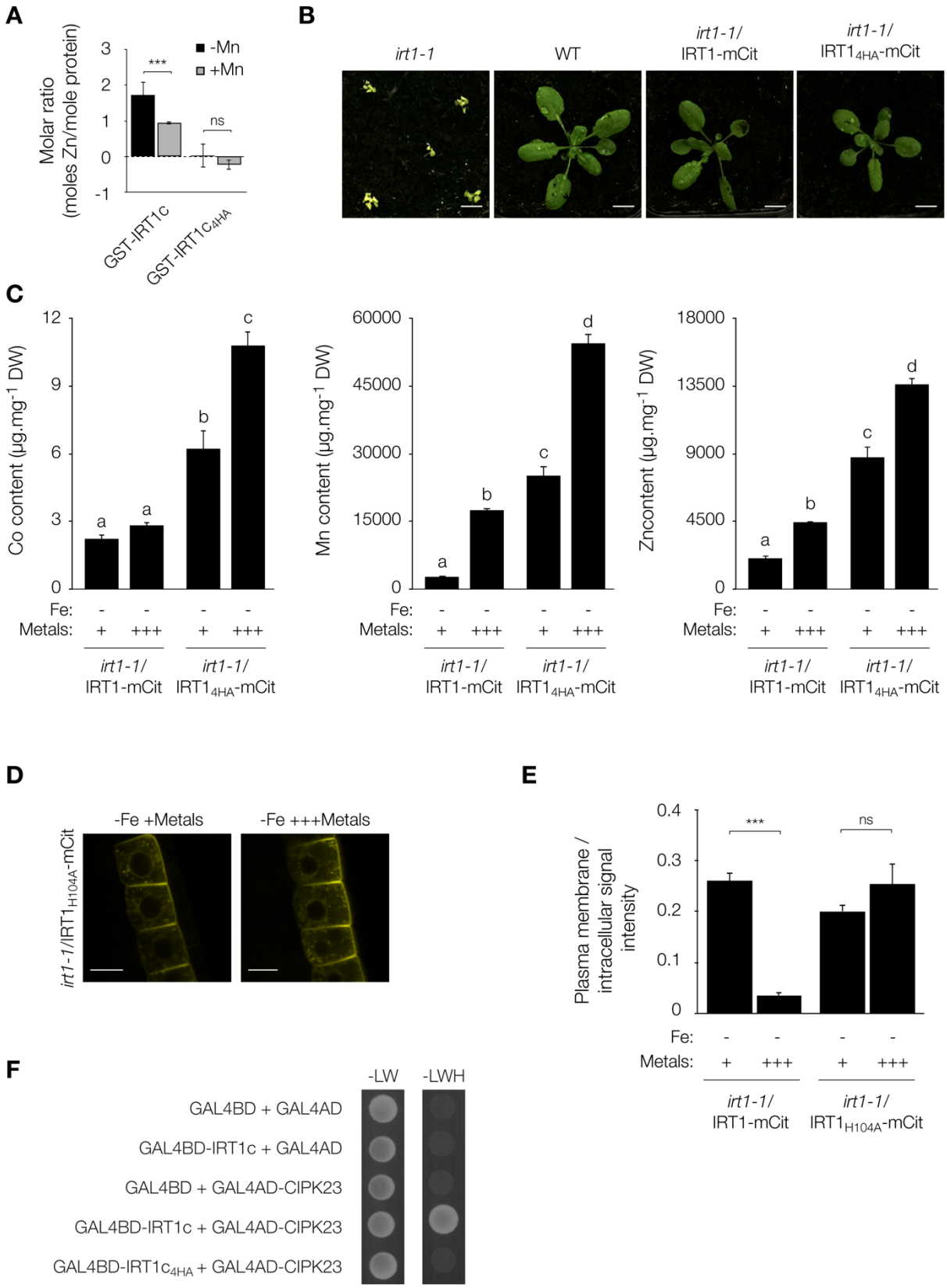

Figure S5. Non-iron metal sensing occurs in the cytoplasm and requires metal transport. Related to Figure 5.

(A) Zinc binding to recombinant IRT1c and IRT1c$_{4HA}$, and competition by manganese. Zinc was detected by atomic absorption spectroscopy. Experiments were carried out in triplicates.

Error bars represent s.d. (n=3). The asterisks indicate significant differences (Mann-Whitney, P<0.0001). **(B)** Phenotypic analyses of wild-type (WT), *irt1-1*, *irt1-1*/IRT1-mCit and *irt1-1*/IRT1$_{4HA}$-mCit plants. Scale bars=1cm. **(C)** Metal content analyses by atomic absorption spectrometry of 12-day-old seedlings described in Figure 5B. Experiments were carried out in triplicates. Error bars represent s.d. (n=3). Different letters indicate means that were statistically different by Tukey's multiple testing method (P<0.05). **(D)** Subcellular localization of the metal transport-deficient IRT1$_{H104A}$-mCit in response to non-iron metal availability in the growth medium. **(E)** Ratio of *irt1-1*/IRT1$_{H104A}$-mCit plasma membrane (PM) to intracellular signal intensities from experiments performed as in (D). The effect of metal nutrition on *irt1-1*/IRT1-mCit is used as control. Experiments were carried out in triplicates on stacks encompassing epidermal cells. Error bars represent standard deviation (s.d. ; n=18). ns, non-significant statistical difference (Mann-Whitney, P>0,05). **(F)** Influence of mutating the metal-binding histidine residues of IRT1 on its interaction with CIPK23, as visualized by yeast two-hybrid.

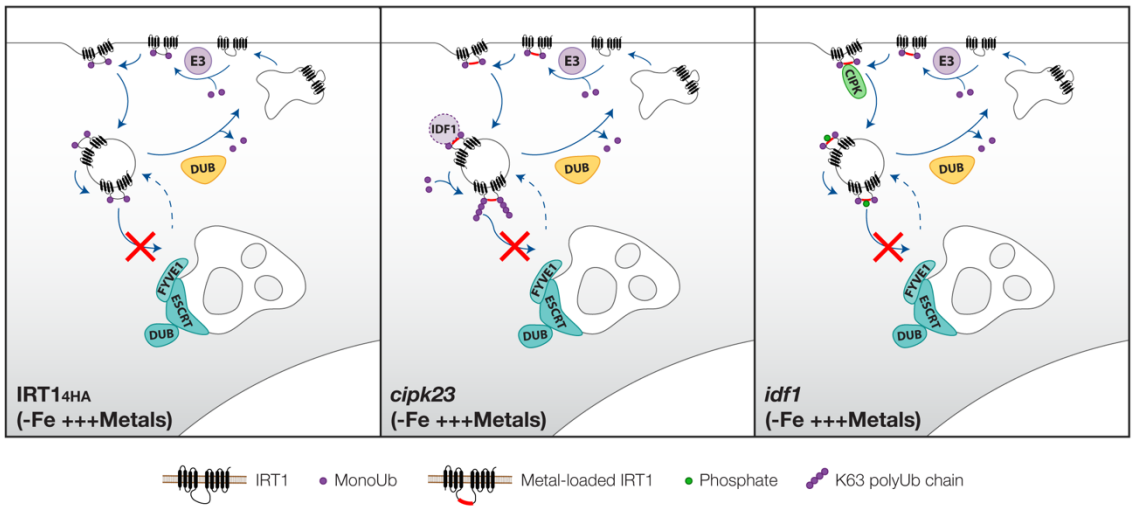

Figure S6. Models illustrating the defects in IRT1 dynamics observed in several mutant backgrounds impaired in non-iron metal excess response. Related to Figure 6.

Metal sensing by the histidine (H)-stretch found in the cytosolic loop of IRT1 is essential for the activation of IDF1 and the recruitment of CIPK23. In $IRT1_{4HA}$-expressing plants (left), the absence of CIPK23-dependent phosphorylation of IRT1 prevents efficient activation and recruitment of IDF1, precluding K63 polyubiquitination of IRT1. This, combined to the absence of phosphorylation of IRT1 itself, or a yet to be characterized ESCRT subunit, blocks the sorting of IRT1 in endosomes yielding PM and EE localization of IRT1.

In *cipk23* (middle), the enhanced interaction between IRT1 and IDF1 upon metal stress is not observed (dashed lines for IDF1). Metal sensing and activation of basal IDF1 levels however operate, allowing low K63 polyubiquitination of IRT1. Such basal K63 polyubiquitinated IRT1 forms build up in the cell due to their inability to reach LE where deubiquitination normally occurs.

In *idf1* (right), IRT1 cannot be K63 polyubiquitinated, preventing its sorting towards LE and the vacuole. DUB, deubiquitinase ; ESCRT, endosomal sorting complex required for transport ; CIPK, CIPK23.

Table S1. List of primers used in this study. Related to STAR Methods.

Cloning

Name	Sequence (5' to 3')
IRT1 attB1	GGGGACAAGTTTGTACAAAAAAGCAGGCTCCATGGCTTCAAATTCAGCACTTC
IRT1 attB2	GGGGACCACTTTGTACAAGAAAGCTGGGTATTAAGCCCATTTGGCGATAATC
IDF1 attB1	GGGGACAAGTTTGTACAAAAAAGCAGGCTTCACCATGTCGATAACGATTCCCTAC
IDF1 attB2	GGGGACCACTTTGTACAAGAAAGCTGGGTAAAAAATTTCACCTTGTGGTCTC
CIPK23 attB1	GGGGACAAGTTTGTACAAAAAAGCAGGCTGGACCATGGCTTCTCGAACAACGCCTTC
CIPK23 attB2	GGGGACCACTTTGTACAAGAAAGCTGGGTATTATGTCGACTGTTTTGCAATTG
IRT1c BamHI	GCGGATCCGACTCCATGGCCACGAGCC
IRT1c EcoRI	GGAATTCTTATCGGTATCGCAAGAGCTG
CIPK23 PstI	CGTGCTGCAGATGGCTTCTCGAACAACGCC
CIPK23 HindIII	CCACAAGCTTCTTATGTCGACTGTTTTGCAATTG

Site-directed mutagenesis

Name	Sequence (5' to 3')
IRT1 H162,164A F	GTTGGTATCATGCCCGCTGGTGCTGGTCATGGTCACGGC
IRT1 H162,164A R	GCCGTGACCATGACCAGCACCAGCGGGCATGATACCAAC
IRT1 H166,168A F	CCCGCTGGTGCTGGTGCTGGTGCCGGCCCCGCAAATGATG
IRT1 H166,168A R	CATCATTTGCGGGGCCGGCACCAGCACCAGCACCAGCGGG
IRT1 K154R F	GCCTATACACCAGCAGGAACGCAGTTGGTATC
IRT1 K154R R	GATACCAACTGCGTTCCTGCTGGTGTATAGGC
IRT1 K179R F	GTTACCTTACCAATAAGAGAAGATGATTCGTC
IRT1 K179R R	GACGAATCATCTTCTCTTATTGGTAAGGTAAC
IRT1 T175D F	CCCGCAAATGATGTTGACTTACCAATAAAAGAAG
IRT1 T175D R	CTTCTTTTATTGGTAAGTCAACATCATTTGCGGG
IRT1 T175A F	CCCGCAAATGATGTTGCCTTACCAATAAAAGAAG
IRT1 T175A R	CTTCTTTTATTGGTAAGGCAACATCATTTGCGGG
CIPK23 K60N F	TGATAATGTCGCTATTAACGTTATTGATAAAGAGAAAG
CIPK23 K60N R	CTTTCTCTTTATCAATAACGTTAATAGCGACATTATCA
CIPK23 T190D F	GTTACTTCACGATACCTGTGGAACA
CIPK23 T190D R	TGTTCCACAGGTATCGTGAAGTAAC

RT-qPCR

Name	Sequence (5' to 3')
EF1a qPCR F	GTCGATTCTGGAAAGTCGAC
EF1a qPCR R	AATGTCAATGGTGATACCACGC
mCit qPCR F	GACTTCTTCAAGTCCGCCATG
mCit qPCR R	GTCCTCCTTGAAGTCGATGC
IRT1 qPCR F	CGGTTGGACTTCTAAATGC
IRT1 qPCR R	CGATAATCGACATTCCACCG